SIDE-CHAIN CHIRAL CENTERS OF AMINO ACIDS AND HELICAL-SCREW HANDEDNESS OF THEIR PEPTIDES

Masakazu Tanaka[1], Masanobu Nagano[1], Yosuke Demizu[1], Kosuke Anan[1], Masaaki Kurihara[2], Mitsunobu Doi[3] and Hiroshi Suemune[1]

[1]Graduate School of Pharmaceutical Sciences, Kyushu University, 812-8582, Fukuoka, Japan, [2]Division of Organic Chemistry, National Institute of Health Sciences, 158-8501, Tokyo, Japan and [3]Osaka University of Pharmaceutical Sciences, 569-1094, Osaka, Japan

Introduction

Helices shown in proteins, as a secondary structure, almost always form right-handed screw sense. The right-handedness of the helix is believed to result from the chiral center at the α-position of proteinogenic L-α-amino acids [1]. Among proteinogenic amino acids, L-isoleucine and L-threonine possess an additional chiral center at the side-chain β-carbon besides the α-carbon. However, only little attention has been paid as to how the side-chain chiral centers affect the secondary structures of their peptides [2]. Recently, we have reported that side-chain chiral centers of chiral cyclic α,α-disubstituted amino acid (*S,S*)-Ac_5c^{dOM} affected the helical secondary structure of its peptides, and the helical-screw direction could be controlled by the side-chain chiral centers without a chiral center at the α-carbon atom (Fig. 1) [3]. Herein we synthesized a chiral bicyclic α,α-disubstituted amino acid, (1*R*,6*R*)-8-aminobicyclo[4.3.0]non-3-ene-8-carboxylic acid {(*R,R*)-$Ab_{5,6=}c$}, and its analogs. Also, we prepared its homopeptides, and studied the relationship between the side-chain chiral centers and the helical-screw handedness of their peptides.

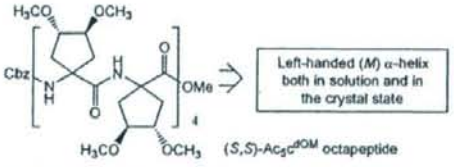

Fig. 1. (S,S)-Ac_5c^{dOM} Octapeptide forming an α-helix.

Results and Discussion:

We designed and synthesized an optically active bicyclic α,α-disubstituted α-amino acid; (*R,R*)-$Ab_{5,6=}c$, in which the α-carbon atom is not a chiral center but the asymmetric centers exist at the side-chain bicyclic skeleton. The amino acid (*R,R*)-$Ab_{5,6=}c$ was synthesized from (*S,S*)-cyclohex-4-ene-1,2-dicarboxylic acid **1** [4] as shown in Fig. 2. The acid (*S,S*)-**1** was converted to a diiodide **2** by reduction and subsequent substitution with iodide. Then, ethyl isocyanoacetate was bisalkylated with **2**, followed by acidic hydrolysis and protection with Boc_2O to give amino acid Boc-[(*R,R*)-$Ab_{5,6=}c$]-OEt (**3**). The olefin in the amino acid **3** could be easily converted to several functional groups. Ozonolysis of the olefin in **3**, followed by

reduction with $NaBH_4$ afforded a dihydroxy amino acid **4** and by oxidation with Oxone® gave a dicarboxylic amino acid **5**, and by reductive amination with $BnNH_2$ produced a bicyclic seven-membered ring amino acid **6**. Furthermore, hydrogenation of the olefin in **3** afforded saturated amino acid Boc-[(*R,R*)-$Ab_{5,6}$c]-OEt **7**. Homopeptides Boc-[(*R,R*)-$Ab_{5,6}$=c]n-OEt (n = 3, 6, 9) were prepared by solution-phase methods, and the six olefin functions in (*R,R*)-$Ab_{5,6}$=c hexapeptide **8** were hydrogenated by H_2/20% $Pd(OH)_2$-C in one step to afford the saturated peptide Boc-[(*R,R*)-$Ab_{5,6}$c]6-OEt **9** in 70% yield.

The IR, ^1H NMR, CD spectra, and the X-ray crystallographic analysis revealed that the (R,R)-$Ab_{5,6}$=c hexapeptide having twelve chiral centers at the side chain forms both diastereomeric right-handed (P) and left-handed (M) 3_{10}-helices. These results are in contrast with the left-handed (M) (*S,S*)-Ac_5c^{dOM} homopeptides controlled by side-chain chiral centers, and suggest that the side-chain chiral environments (bulkiness or flexibility) might be important for the control of the helical-screw handedness [5].

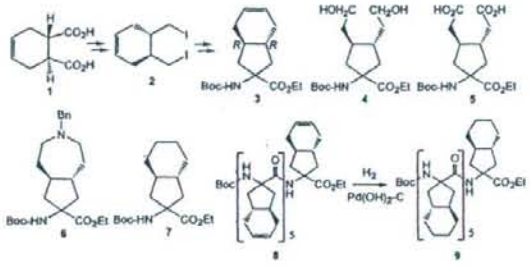

Fig. 2. Synthesis of chiral bicyclic and cyclic α,α-disubstituted α-amino acids, and their peptides.

Acknowledgements

This work was supported in part by Grants-in-Aid for Scientific Research from the Japan Society for the Promotion of Science, and also by Travel Grant from the JSPS.

References

1. Branden, C. and Tooze, J., In: Introduction to Protein Structure, Garland, New York, 1991, p. 1.
2. Widmer U., Lorenzi G. P.and P. Pino, Biopolymers, 18 (1979) 239.; Toniolo C., Bonora G. M.and S. Salardi, Int. J. Biol. Macromol., 3 (1981) 377.
3. Tanaka M., Demizu Y., Doi M., Kurihara M.and H. Suemune, Angew. Chem. Int. Ed., 43 (2004) 5360.
4. Bernardi A., Arosio D., Dellavecchia D.and F. Micheli, Tetrahedron: Asymmetry, 10 (1999) 3403.
5. Tanaka M., Anan K., Demizu Y., Kurihara M., Doi M. and H. Suemune, J. Am. Chem. Soc., 127 (2005) 11570.

CONTROLLING THE HELICAL SECONDARY STRUCTURE OF HETEROPEPTIDES USING CHIRAL CYCLIC α,α-DISUBSTITUTED AMINO ACIDS

Masanobu Nagano[1], Masakazu Tanaka[1], Yosuke Demizu[1], Masaaki Kurihara[2], Mitsunobu Doi[3] and Hiroshi Suemune[1]

[1]Graduate School of Pharmaceutical Science, Kyushu University, 812-8582, Fukuoka, Japan, [2]National Institute of Health Sciences, 158-8501, Tokyo, Japan and [3]Osaka University of Pharmaceutical Sciences, 569-1094, Osaka, Japan

Introduction

Helical structures in proteins almost always form a right-handed (*P*) helical-screw sense, which is believed to result from the asymmetric center at the α-position of L-α-amino acids [1]. Besides an asymmetric center at the α-position, L-Ile and L-Thr possess an additional chiral center at the side-chain β-position. However, only a little attention has been paid as to how the asymmetric center at the side chain affects the secondary structure of peptides. We have previously reported that chiral cyclic α,α-disubstituted amino acid (*S,S*)-$Ac_5c^{d()M}$, in which the α-carbon is not a chiral center but the asymmetric centers exist at the side chain cyclopentane, could control the helical-screw direction of its homopeptides into the left-handedness [2]. Herein we synthesized heteropeptides containing (*S,S*)-$Ac_5c^{d()M}$ in Aib sequences, and also peptides containing four various disubstituted amino acids in L-Leu sequences. The Aib is an achiral amino acid, and thus does not have a bias for the helical-screw handedness, while the L-Leu has an asymmetric center at the α-position and has a property for β-sheet or helix formation [3]. Furthermore, we studied the preferred secondary structures of these peptides, and effect of the Ac_5c^{dOM} on the conformation.

Fig. 1. X-ray structure of (S,S)-Ac_5c^{dOM} octapeptide

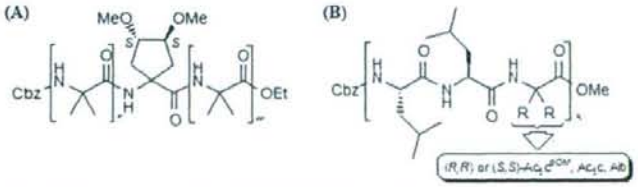

Fig. 2. Structure of heteropeptides; (A) Aib heteropeptides and (B) Leu heteropeptides

Results and Discussion

Both enantiomers of chiral cyclic α,α-disubstituted amino acids Ac_5c^{dOM} were synthesized starting from dimethyl L-(+)- and D-(-)-tartrate, according to our previous report [2]. The chiral cyclic amino acid was incorporated into Aib sequence by solution-phase methods; the (*S,S*)-Ac_5c^{dOM} was introduced to the N-terminal, to the C-terminal, and at the center position of Aib peptides. Conformational analysis by using the ^{1}H NMR, FT-IR, and X-ray crystallographic analysis revealed that dominant conformation of the Aib peptides containing a chiral cyclic (*S,S*)-Ac_5c^{dOM} was 3_{10}-helix both in solution, and in the solid state. However, the control of helical-screw handedness by one chiral (*S,S*)-Ac_5c^{dOM} in Aib sequences seemed to be difficult. Also, we incorporated the achiral or chiral disubstituted amino acids into L-Leu sequences. Conformation analysis by using CD, ^{1}H NMR, and FT-IR spectra disclosed that the dominant conformation of heteropeptides containing the chiral cyclic Ac_5c^{dOM} in L-Leu sequences was the right-handed (*P*) helical structure, due to the chiral centers at the α-position of L-α-amino acid. The detailed conformation analysis including the X-ray crystallographic analysis will be reported elsewhere.

Acknowledgements

This work was supported in part by Grants-in-Aid for Scientific Research from the Japan Society for the Promotion of Sciences, and also by Travel Grant from the Kyushu University Foundation and from the Japanese Peptide Society.

References

1. Branden, C. and Tooze, J., In: Introduction to Protein Structure, Garland, New York, 1991, p. 1.
2. Tanaka M., Demizu Y., Doi M., Kurihara, M. and H. Suemune, Angew. Chem. Int. Ed., 43 (2004) 5360; Toniolo C., Bonora G, M., Palumbo M. and E. Peggion, Biopolymers, 17, (1978) 1713.

Design and Screening Strategies for α-Glucosidase Inhibitors Based on Enzymological Information

Wataru Hakamata[1],*, Masaaki Kurihara[2], Haruhiro Okuda[2], Toshiyuki Nishio[1] and Tadatake Oku[1]

[1]*Department of Biological Chemistry, College of Bioresource Sciences, Nihon University,* [2]*Division of Organic Chemistry, National Institute of Health Sciences (NIHS)*

Abstract: α-glucosidase inhibitors are marketed as therapeutic drugs for diabetes that act through the inhibition of carbohydrate metabolism. Inhibitors of the α-glucosidases that are involved in the biosynthesis of *N*-linked oligosaccharide chains have been reported to have antitumor, antiviral, and apoptosis-inducing activities, and some have been used clinically. α-Glucosidase inhibitors have interesting biological activities, and their design, synthesis, and screening are being actively performed. In quite a few reports, however, α-glucosidases with different origins than the target α-glucosidases, have been used to evaluate inhibitory activities. There might be confusion regarding the naming of α-glucosidases. For example, the term α-glucosidase is sometimes used as a generic name for α-glucoside hydrolases. Moreover, IUBMB recommends the use of "α-glucosidase" (EC 3.2.1.20) for exo-α-1,4-glucosidases, which are further classified into four families based on amino acid sequence similarities. Accordingly, substrate specificity and susceptibility to inhibitors varies markedly among enzymes in the IUBMB α-glucosidases. The design and screening of inhibitors without consideration of these differences is not efficient. For the development of a practical inhibitor that is operational in cells, HTS using the target α-glucosidase and the computer-aided design of inhibitors based on enzymatic information concerning the same α-glucosidase are essential.

Keywords: α-glucosidase, substrate specificity, inhibitor, HTS, virtual screening, *in silico*, structure based drug design.

INTRODUCTION

Inhibitors of small intestinal α-glucoside hydrolases were revealed to improve postprandial hyperglycemia in the 1970s and were approved as therapeutic drugs for diabetes in the 1990s. Recently, sugar chains have been attracting attention as a third class of biopolymer following nucleic acids and proteins, and now the elucidation of sugar chain functions is indispensable in postgenomic studies. This is because glycoproteins and glycolipids play important roles in many biotic phenomena, such as embryogenesis, differentiation, cancer, infection, inflammation, aging, reproduction, and regeneration. Accordingly, the *N*-linked oligosaccharide processing enzymes, e.g., glycosidases or glycosyltransferases have emerged as new molecular targets in drug development studies. Inhibitors of these enzymes are seen as potential drug seeds as well as tools for the elucidation of biotic phenomena. In this review, we survey the classification of the α-glucoside hydrolases involved in carbohydrate metabolism and *N*-linked oligosaccharide biosynthesis, detailing differences in their nomenclature, reaction mechanisms, and substrate specificity. In addition, the construction of a HTS system for α-glucosidase inhibitors and *in silico* inhibitor design and screening based on the three-dimensional structures of α-glucosidases are described.

*Address correspondence to this author at the 1866 Kameino, Fujisawa, Kanagawa 252-8510, Japan; Tel/Fax: +81-466-84-3960;
E-mail: hakamata.wataru@nihon-u.ac.jp

Classification of α-Glucosidases and Related Enzymes

The CAZy database [1] classifies carbohydrate-related enzymes based on amino acid sequence similarities [2-5]. In CAZy, most α-glucosidases (EC 3.2.1.20) are classified into GH13 and GH31, and the others are classified into GH4 and GH97. ER processing α-glucosidase I (EC 3.2.1.106, official name: Mannosyl-oligosaccharide glucosidase) and ER processing α-glucosidase II (EC 3.2.1.84, official name: Glucan 1,3-α-glucosidase) are known as *N*-linked oligosaccharide processing enzymes and are classified into GH63 and GH31, respectively. These enzymes are exo-type glycosidases that hydrolyze α-D-glucopyranoside linkages. During the hydrolysis of α-glucosidases, the GH13 and GH31 α-glucosidases release α-D-glucopyranose with retention of the configuration in the anomeric position [6,7], and processing α-glucosidase I releases β-D-glucopyranose and causes inversion of the configuration [8]. The anomeric configuration of D-glucopyranose released by processing α-glucosidase II has not been identified. Glucoamylase (EC 3.2.1.3) is part of a group of enzymes that hydrolyze α-glucopyranosides from the non-reducing end in an exo-type manner and release β-D-glucopyranose. Its reaction mechanism is different from that of α-glucosidases (EC 3.2.1.20) and it should be strictly distinguished from them. The CAZy classificationof α-glucosidases and related enzymes, reaction types, and the anomeric configurations of the products produced are summarized in Table **1**. Furthermore, commercially available α-glucosidases are classified according to their GH number in CAZy as shown in Table **2**.

1568-0266/09 $55.00+.00

Table 1. Classification of α-Glucosidase and Related Enzymes

Official Name	E.C. Number	Glycoside Hydrolase Family Number	Product	Anomeric Configuration
α-Glucosidase	3.2.1.20	4, 13, 31, 97	α-Glucose	Retain
Mannosyl-oligosaccharide glucosidase	3.2.1.106	63	β-Glucose	Inversion
Glucan 1,3-α-glucosidase	3.2.1.84	31	Unknown	Unknown
Oligo-1,6-glucosidase	3.2.1.10	4, 13, 31	α-Glucose	Retain
Sucrose α-glucosidase	3.2.1.48	31	α-Glucose	Retain
β-Fructofuranosidase	3.2.1.26	32, 68, 100	α-Glucose	Retain
Glucan 1,4-α-glucosidase	3.2.1.3	15	β-Glucose	Inversion

Table 2. Glycoside Hydrolase Family Number of Commercially Available α-Glucosidases

Origin	Glycoside Hydrolase Family Number	Supplier
S. cerevisiae	13	Sigma
B. stearothermophilus	13	Sigma
A. niger	31	Megazyme
Rice	31	Sigma

α-Glucosidases (EC 3.2.1.20) are also known by other names: maltase, acid maltase, glucoinvertase, glucosidosucrase, lysosomal α-glucosidase, and maltase-glucoamylase. Enzymes corresponding to α-glucosidase include oligo-1,6-glucosidase (EC 3.2.1.10) and sucrose α-glucosidase (EC 3.2.1.48), and also these are called isomaltase and sucrase, respectively. α-Glucosidase and related enzymes have various other names. These similar names sometimes cause confusion in the interpretation and evaluation of research results. Official names and alternative names of α-glucosidase and related enzymes are summarized in Table **3**.

Acquisition of the Enzymological Information of α-Glucosidases for Inhibitor Design using Synthetic Small Molecules

In some reports, α-glucoside hydrolases, which include all the enzymes that cleave α-D-glucopyranoside bonds in an exo-type manner and release glucose, and the specific α-glucosidases (EC 3.2.1.20) are mentioned as if they were identical, and inhibitor designs seem to be based on the enzymes different from those used in the assays. For example, some α-glucosidase inhibitors were designed and synthesized for use as antiviral drugs that would block *N*-linked oligosaccharide processing in host cells, but these were evaluated using the α-glucosidase from yeast (*S. cerevisiae*) and/or other sources. The yeast α-glucosidase belongs to GH13, whereas the targets of antiviral drugs are processing α-glucosidases I and II. These evaluations are inadequate for discovery of processing α-glucosidase I and II inhibitors, even if the inhibitors a thoroughly designed. It is not unusual that strong yeast α-glucosidase inhibitors often exhibit few effects toward mammalian cells, though this may also be related to the transferability of the inhibitors into cells. In other words, a low inhibitory activity against yeast α-glucosidase does not necessarily translate into low activity against processing α-glucosidase I and II. For example, a typical α-glucosidase inhibitor, 1-deoxynojirimycin, inhibits yeast α-glucosidases (IC_{50} = 12.6 μM [9]) *in vitro*. However, 1-deoxynojirimycin has very weak effects against BVDV, which serves as a model organism for HCV at the cellular level [10]. The potent α-glucosidase inhibitor kojibiose type pseudodisaccharide and its derivatives show low IC_{50} values (120 nM - 3.1 μM) and have no effect against processing glucosidases [11].

We have examined the substrate specificity of α-glycosidases for inhibitor design using small synthetic molecules [12-21], some of which are summarized in Fig. (**1**). Among the α-glucosidases, the GH31 α-glucosidases (from rice, *A. niger*, flint corn, and sugar beet) and processing α-glucosidase II (from rat liver microsomes) possessed α-2-deoxy-glucosidase activity, and this activity was about twice as high as their the α-glucosidase activity. The C-2 hydroxyl groups of the glycons are not essential for the hydrolysis action of the GH31 α-glucosidases and processing α-glucosidase II, while GH13 α-glucosidases (*S. cerevisiae*, *B. stearothermophilus*, and honeybee isozyme I, II, and III) all require the hydroxyl groups of the glycons for their hydrolyzing activity. α-Mannosidases from jack beans

Table 3. Official Name and Alternative Name of α-Glucosidase and Related Enzymes

Official Name	E.C. Number	Alternative Name (s)
α-Glucosidase	3.2.1.20	Maltase, Acid maltase, Glucoinvertase, Glucosidosucrase Lysosomal α-glucosidase, Maltase-glucoamylase
Mannosyl-oligosaccharide glucosidase	3.2.1.106	Processing α-glucosidase I, Glucosidase I
Glucan 1,3-α-glucosidase	3.2.1.84	Processing α-glucosidase II, Glucosidase II, Exo-1,3-α-glucanase
Oligo-1,6-glucosidase	3.2.1.10	Isomaltase, Oligosaccharide α-1,6-glucosidase Sucrase-isomaltase
Sucrose α-glucosidase	3.2.1.48	Sucrase, Sucrase-isomaltase, Sucrose α-glucohydrolase
β-Fructofuranosidase	3.2.1.26	β-Fructosidase, Invertase, Saccharase
Glucan 1,4-α-glucosidase	3.2.1.3	Glucoamylase, 1,4-α-D-Glucan glucohydrolase Amyloglucosidase, Exo-1,4-α-glucosidase γ-Amylase, Lysosomal α-glucosidase

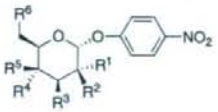

Glucopyranoside derivatives
1: R^1=OH, R^2=H, R^3=OH, R^4=OH, R^5=H, R^6=OH (PNP Glc)
2: R^1=R^2=H, R^3=OH, R^4=OH, R^5=H, R^6=OH (PNP 2D Glc)
3: R^1=OH, R^2=R^3=H, R^4=OH, R^5=H, R^6=OH (PNP 3D Glc)
4: R^1=OH, R^2=H, R^3=OH, R^4=R^5=H, R^6=OH (PNP 4 D Glc)
5: R^1=OH, R^2=H, R^3=OH, R^4=OH, R^5=R^6=H (PNP 6D Glc)

Mannopyranoside derivatives
6: R^1=H, R^2=OH, R^3=OH, R^4=OH, R^5=H, R^6=OH (PNP Man)
2: R^1=R^2=H, R^3=OH, R^4=OH, R^5=H, R^6=OH (PNP 2D Man)
7: R^1=H, R^2=OH, R^3=H, R^4=OH, R^5=H, R^6=OH (PNP 3D Man)
8: R^1=H, R^2=OH, R^3=OH, R^4=R^5=H, R^6=OH (PNP 4 D Man)
9: R^1=H, R^2=OH, R^3=OH, R^4=OH, R^5=R^6=H (PNP 6D Man)

Galactopyranoside derivatives
10: R^1=OH, R^2=H, R^3=OH, R^4=H, R^5=OH, R^6=OH (PNP Gal)
11: R^1=R^2=H, R^3=OH, R^4=H, R^5=OH, R^6=OH (PNP 2D Gal)
12: R^1=OH, R^2=R^3=R^4=H, R^5=OH, R^6=OH (PNP 3D Gal)
4: R^1=OH, R^2=H, R^3=OH, R^4=R^5=H, R^6=OH (PNP 4 D Gal)
13: R^1=OH, R^2=H, R^3=OH, R^4=H, R^5=OH, R^6=H (PNP 6D Gal)

Fig. (1). Synthetic Small molecules as substrates for profiling the molecular recognition of α-glucosidase.

and almonds had α-6-deoxy-mannosidase activity levels equivalent to their α-mannosidase activitiy levels. Among the α-galactosidases, α-galactosidase from green coffee beans and *M. vinacea* had weak α-2-deoxy-galactosidase and α-6-deoxy-galactosidase activity, and *A. niger* α-galactosidase showed α-2-deoxy-galactosidase activity with a strength twice as great as its α-galactosidase activity. These results are summarized in Table **4**. The specificities for the deoxyglycons varied markedly throughout the different glycosidase families, while each family retained its original glycon specificity, strongly indicating that the major differences between the α-glucosidase family are due to the residues in the glycon recognition sites (subsite -1) in Fig. (**2**).

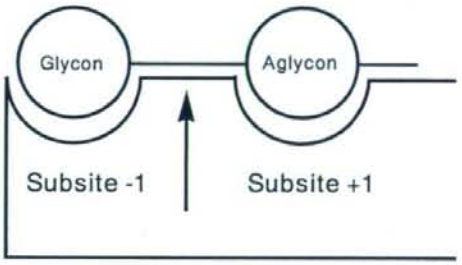

Fig. (2). Schematic diagram of substrates bound to the α-glucosidase subsite. Hydrolysis, shown by an arrow, takes place between subsites -1 and +1.

α-Glucosidases as Molecular Targets for Drug Discovery

Therapeutic drugs for type 2 diabetes, such as acarbose (Bayer), miglitol (Bayer), and voglibose (Takeda) in Fig. (**3**), inhibit small intestinal α-glucoside hydrolases (gluco-amylase (EC 3.2.1.3), sucrase (EC 3.2.1.48), and α-glucosidase (EC 3.2.1.20) [22]. These drugs only affect postprandial glucose levels and do so by competitively inhibiting the binding of oligosaccharides to the α-glucoside hydrolases. These enzymes cleave oligosaccharides to monosaccharides, which can then be absorbed. Thus, when taken with the first bite of food, these agents delay the absorption of carbohydrates. These are the first-line drugs for type 2 diabetes, and their importance is very high [23]. They are particularly important because the cost of diabetes to the United States healthcare system amounts to $100 billion in direct and indirect expenditure annually [24].

Table 4. Relative Rates of Hydrolysis of Monodeoxy Substrates Using α-Glycosidases [9-11, 13-14]

Enzyme / Substrate	Relative Rate of Hydrolysis (%)				
	PNP Glc (1)	PNP 2D Glc (2)	PNP 3D Glc (3)	PNP 4D Glc (4)	PNP 6D Glc (5)
α-Glucosidase					
S. cerevisiae (GH13)	100	–	–	–	–
B. stearothermophilus (GH13)	100	–	–	–	–
Honeybee I (GH13)	100	–	–	–	–
Honeybee II (GH13)	100	–	–	–	–
Honeybee III (GH13)	100	–	–	–	–
Rice (GH31)	100	175	–	–	–
Sugar beet (GH31)	100	244	–	–	–
Flint corn (GH31)	100	231	3.7	–	–
A. niger (GH31)	100	259	11.9	–	–
Processing α-glucosidase II Rat liver microsome (GH31)	100	189	–	–	–
Enzyme / Substrate	Relative rate of hydrolysis (%)				
	PNP Man (**6**)	PNP 2D Man (**2**)	PNP 3D Man (**7**)	PNP 4D Man (**8**)	PNP 6D Man (**9**)
α-Mannosidase					
Canavalia ensiformis (Jack bean, GH38)	100	–	–	–	92.2
Prunus dulcis (Almond)	100	–	–	–	118
Enzyme / Substrate	Relative rate of hydrolysis (%)				
	PNP Gal (**10**)	PNP 2D Gal (**11**)	PNP 3D Gal (**12**)	PNP 4D Gal (**4**)	PNP 6D Gal (**13**)
α-Galactosidase					
Green coffee bean	100	15.0	–	–	3.3
M. vinacea (GH27)	100	19.0	–	–	8.8
A. niger (GH27)	100	230	–	–	–

Relative rate of hydrolysis is expressed by comparison with the amount of *p*-nitrophenol released from PNP Glc (**1**), PNP Man(**6**), and PNP Gal (**10**), respectively which is taken as 100%. – : Hydrolytic activity was not detected.

Inhibitors of *N*-linked oligosaccharide processing α-glucosidases I and II have various useful physiological and biological activities. *N*-Linked oligosaccharides are attached to many nascent proteins as posttranslational modifications. The formation of the *N*-linked oligosaccharide chains in the ER starts with the attachment of $Glc_3Man_9GlcNAc_2$ to a nascent protein and removal of the glucose residues by processing α-glucosidases I and II [25,26]. The involvement of the processing of glucose and mannose residues in quality control [27,31] and ERAD [32-35] of glycoproteins in the ER has recently been clarified. Inhibitors of processing α-glucosidase I and II and the other *N*-linked oligosaccharide chain processing enzymes disturb protein folding and intracellular transport by inhibiting *N*-linked oligosaccharide chain formation [36,37] causing antitumor activities [38,44], antiviral activities (HIV [45-46], HCV [47-48], HBV [49], influenza [50], SARS [51,52], etc. [53]), and apoptosis induction [54,55]. The destruction caused by ERAD is considered to be a major cause of neurodegenerative diseases such as Alzheimer's disease and Parkinson's disease [56], and *N*-linked oligosaccharide chain processing enzymes have been attracting attention as molecular targets for new drug development [57,59].

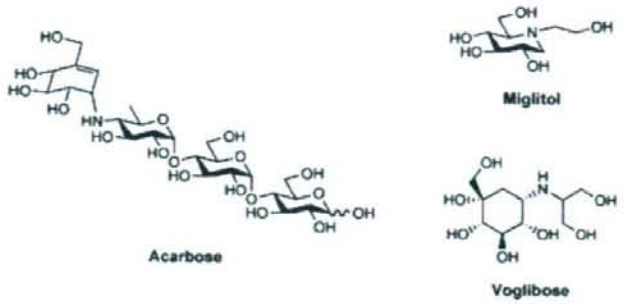

Fig. (3). Chemical structures of drugs for type 2 diabetes.

Characteristics of α-Glucosidase Inhibitors

Forty years have passed since the most renowned glucosidase inhibitor, nojirimycin, was first reported in 1966 [59,62]. Since then, an enormous number of glucosidase inhibitors have been discovered, synthesized, and have had their inhibitory activities investigated [64-73].

The reported α-glucosidase inhibitors have some of the following characteristics: (1) sugar (substrate)-mimic structures, (2) the ability to form ionic bonds with nucleophilically catalyzing residues, (3) transition-state-like structures, (4) the ability to form hydrogen bonds with catalytic acid residues, (5) the ability to make ionic and hydrophobic interactions at sites other than the active site, and (6) the ability to form covalent bonds with enzymes through an epoxy or aziridine group. Archetypal examples are summarized in Fig. (**4**). These model structures are reported to be potent inhibitors that combine the above-mentioned (1)-(6) features. The target of these α-glucosidase inhibitors is the glycon binding subsite (subsite -1) of α-glucosidases. However, non-sugar-mimicking α-glucosidase inhibitors have recently been reported (Fig. (**5**)) [74-76] and these inhibitors might bind to the aglycon binding site or elsewhere.

HTS of α-Glucosidase Inhibitors

The major target enzymes of the α-glucosidase in drug development are the small intestinal α-glucosidases involved in the carbohydrate metabolic system and the processing α-glucosidases I and II involved in *N*-linked oligosaccharide chain processing. To obtain inhibitor leads, HTS toward the glycosidases has been aggressively carried out and reported in recent years [77,79]. To establish practical HTS methods for these enzymes, the use of the target α-glucosidase and substrate selection are important. In view of the advances in molecular biology, it is not difficult to prepare active enzymes by expressing human-derived target enzymes. The substrates should be selected carefully with consideration of the markedly different specificities of the target enzymes [80,87]. Generally, GH13 α-glucosidases exhibit high hydrolytic activity toward monosaccharide substrates, but GH31 α-glucosidases and processing α-glucosidase I and II show higher hydrolytic activity toward oligosaccharides than monosaccharides. α-Glucopyranosides with a chromophores

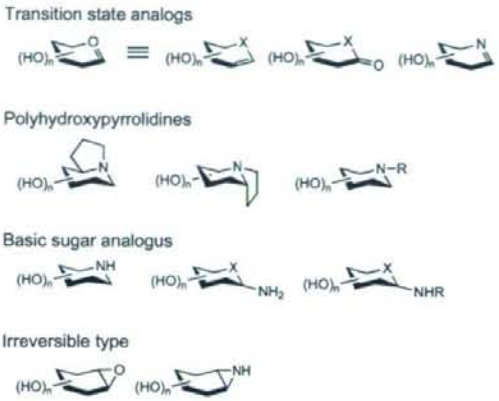

Fig. (4). Classification of typical α-glucosidase inhibitors [64].

or fluorophores conjugated at the anomeric positions are widely used as substrates. Their activities can be measured simply and sensitively using these substrates; however, these substrates are still insufficient because large amounts of enzyme are necessary to measure GH31 α-glucosidases and processing α-glucosidase II activity owing to their low specificity toward mono-saccharides [88]. The reported α-glucosidase inhibition activity measurements have paid little attention to the amounts or activity units of the enzymes. The activity of the GH31 α-glucosidases was measured using more than ten times the amount of enzyme used for measuring the activity of the GH13 α-glucosidases. We developed PNP α-D-2-deoxy-glucopyranoside (**2**) as a highly specific substrate for GH31 α-glucosidases and processing α-glucosidase II and found that the activity of 2 as twice as high as that of PNP α-D-glucopyranoside (**1**) [14]. We are developing a chromophoric monosaccharide substrate for processing α-glucosidase II with a higher specific activity. A 20% reduction in the amount of enzyme required has been accomplished by this method. Although processing α-glucosidase I is an important molecular target for drug development to the best of our knowledge, there have been no previous reports on the development of a substrate for processing α-glucosidase I for use in HTS. Unlike GH13 α-

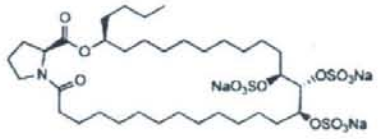

Penarolide sulfate A_1, IC_{50} = 1.2 μg / mL. [73]

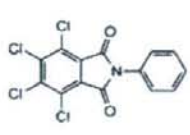

CP0P, IC_{50} = 2.6 μM. [74]

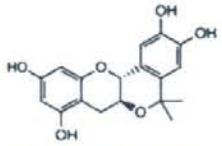

PC1, IC_{50} = 0.7 μM. [75]

Fig. (5). Chemical structures of non-sugar-mimicking α-glucosidase inhibitors [73-75].

glucosidase, processing α-glucosidase I does not use monosaccharide derivatives as its substrate, but instead is inhibited by monosaccharide substrates [14, 89]. A simple processing α-glucosidase I assay method has been reported [14, 90,91], but it is not appropriate for HTS because it requires impractical materials such as a virus as the substrate and a radioisotope for the reaction tracing. We analyzed the molecular recognition of subsite -1 of processing α-glucosidase I using synthetic small molecules [14], but have not been able to develop a substrate adequate for HTS. Development of HTS for processing α-glucosidase I is an important issue and urgent resolution is needed.

In silico Techniques used in Computer Aided Molecular Design and Virtual Screening of α-Glucosidase Inhibitors

Computer-aided molecular design, "*in silico* molecular design", and computer ligand screening "*in silico* virtual screening", have recently become important with the rapid increase in the information available concerning three-dimensional protein structures and the development of high-speed computer-processing technologies. *In silico* molecular design is essential for the structural optimization of the active compounds obtained by HTS. *In silico* virtual screening of real (commercial and house) and virtual libraries and the molecular design of compounds that fit the ligand binding domain of a target protein have been effectively used to develop inhibitors [92,94].

In 2004-2006, the three-dimensional structures of the GH31 α-glucosidases *S. solfataricus* α-glucosidase (PDB ID: 2G3M and 2G3N) [95] and GH31 α-glycosidase YicI (PDB ID: 1XSI, 1XSJ, and 1XSK) [96] as well as *E. coli* α-xylosidase (PDB ID: 1WE5 [97] and 2F2H [98]) were solved. An *E. coli* α-xylosidase with an α-glucosidase activity was prepared by a mutation of its active site [99, 100]. The structure of *S. solfataricus* α-glucosidase shows differences from that of the other GH31 α-glucosidase, the *E. coli* α-xylosidase, although the enzymes have similar $(\beta/\alpha)_8$ barrels. For the main frame of GH13 α-glucosidase *in silico*, the structure of *B. cereus* oligo-1,6-glucosidase (EC. 3.2.1.10, isomaltase, PDB ID: 1UOK) [101] has been generally used. Fig. (**6**) shows the three-dimensional structures of a GH13 α-glucosidase (1UOK) and two GH31 α-glucosidases (2G3N and 1WE5). The three-dimensional structures of processing α-glucosidases I and II have not yet been reported.

An *in silico* molecular design of a glycosidase inhibitor is carried out by calculating the minimum interaction energies between a ligand and the active site of an enzyme. The most successful case of this method was performed for a marketed anti-influenza agent, Zanamivir, which acts through the inhibition of an influenza virus neuraminidase [103,107]. Clarification of the three-dimensional structure of enzymes enables the evaluation of existing inhibitors and the theoretical design of novel inhibitors. Before *in silico* technologies, many articles discussed the necessity of the SBDD approach, and their importance has increased. For the *in silico* design of α-glucosidase inhibitors using the three-dimensional structures of α-glucosidases, the following methods are applicable: (1) Structural optimization of existing inhibitors, (2) screening of real and virtual compound libraries by docking simulations, and (3) *de novo* design of inhibitors that bind to enzyme active sites, and several papers have reported virtual screening of α-glucosidase inhibitors [108-110]. Methods (2) and (3) will allow for the discovery of structurally novel inhibitors while such inhibitors have been previously discovered mainly from natural occurring substances. In the near future, computer simulations aimed at SBDD will produce excellent inhibitors in the virtual world. One of the current difficulties with *in silico* molecular design resides in the algorithm for the induced-fit phenomena of enzymes. Development of the algorithm is underway, and the design of inhibitors in consideration of induced-fit will be possible in the near future [111,112].

Summary and Discussion

New pieces of information on the functions of oligosaccharides in glycoproteins and glycolipids are reported frequently, expanding the potential physiological roles of α-

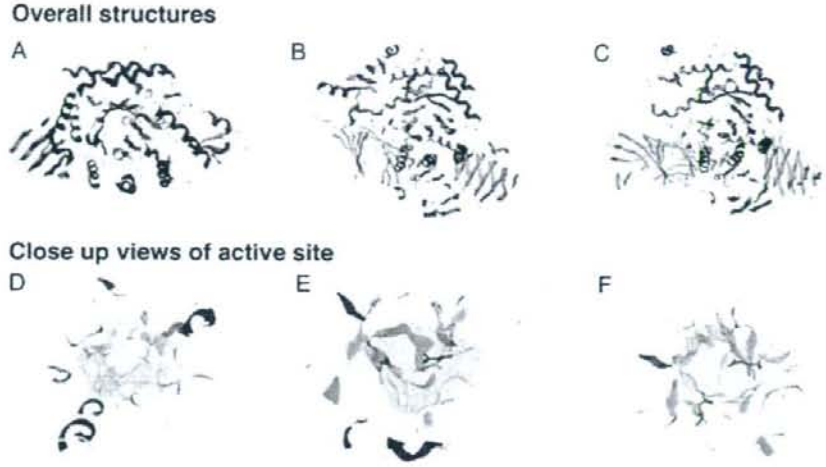

Fig. (6). Crystal structures of *B. cereus* oligo-1,6-glucosidase (A and D, 1UOK; belonging to GH13), *S. solfataricus* α-glucosidase (B and E, monomer structure, 2G3N; belonging to GH31), and *E. coli* α-xylosidase (C and F, monomer structure, 1WE5; belonging to GH31). The $(\beta/\alpha)_8$ barrels are shown using ribbon representations with green β-strands, red α-helices, and white coil segments. The cavities of active sites are represented in gray. The catalytic nucleophile and acid/base residues are shown as stick models in red. The figure was produced using Chemical Computing Inc's Molecular Operating Environment (MOE) version 2007.0901 [102].

glucosidase inhibitors. The importance of *N*-linked oligosaccharide processing enzyme inhibitors has been increasing not only as molecular targets in the development of new drugs but also as tools for the elucidation of biotic phenomena.

Many reports concerning the design, synthesis, and screening of α-glucosidase inhibitors have paid little attention to the classification and multiple naming of α-glucosidases or the differences in the molecular recognitions and three-dimensional structures of α-glucosidases. However, precise molecular designs based on the three-dimensional structures of α-glucosidases require close observation of molecule-enzyme interactions. No assay systems meeting HTS demands have been established for processing α-glucosidase I and II or the other *N*-linked oligosaccharide processing enzymes despite the increasing importance of these enzymes and their inhibitors from chemical biological viewpoints. The establishment of a HTS system for inhibitory activity evaluations using target enzymes and suitable substrates will provide abundant information on the structure-activity relationship, and *in silico* molecular design and screening based on this information and enzyme three-dimensional structural information will lead to the discovery of compounds with novel chemical structures, inhibitory mechanisms, and inhibitory activities. Furthermore, the elucidation of biotic phenomena and the development of novel drugs using these inhibitors is expected.

ACKNOWLEDGMENTS

This research was partly supported by the Ministry of Education, Science, Sports and Culture, Grant-in-Aid for Young Scientists (B)(No. 17790097) to W. H. and Health and Labour Sciences Research Grants for Research on HIV/AIDS to W. H. from the Ministry of Health, Labour and Welfare, Japan.

ABBREVIATIONS

HTS	=	High throughput screening
IUBMB	=	International Union of Biochemistry and Molecular Biology
CAZy	=	Carbohydrate-active enzymes
GH	=	Glycoside hydrolase family
ER	=	Endoplasmic reticulum
BVDV	=	Bovine viral diarrhea virus
HCV and HBV	=	Hepatitis C and B virus
HIV	=	Human immunodeficiency virus
SARS	=	Severe acute respiratory syndrome
S. cerevisiae	=	*Saccharomyces cerevisiae*
A.	=	*Aspergillus*
B.	=	*Bacillus*
M.	=	*Mortirella*
S. solfataricus	=	*Sulfolobu solfataricus*
E.	=	*Escherichia*
ERAD	=	Endoplasmic reticulum-associated degradation
PNP	=	*p*-nitrophenyl
SBDD	=	Structure based drug design

REFERENCES

[1] Consult http://www.cazy.org/CAZY/ for further information.

[2] Coutinho, P. M.; Henrissat, B. Carbohydrate-Active Enzymes: an Integrated Approach. In *Recent Advances in Carbohydrate Engineering*; Gilbert H. J.; Davies G. J.; Svensson, B.; Henrissat, B.; Eds. Royal Society of Chemistry, **1999**, pp 3-12.

[3] Davies, G. J.; Gloster, T. M.; Henrissat, B. Recent structural insights into the expanding world of carbohydrate-active enzymes. *Curr. Opin. Struct. Biol.* **2005**, *15*, 637-645.

[4] Henrissat, B. A Classification of Glycosyl Hydrolases Based on Amino Acid Sequence Smilarities. *Biochem. J.* **1991**, *280*, 309-316.

[5] Henrissat, B.; Bairoh, A. New families in the classification of glycosyl hydrolases based on amino acid sequence similarities. *Biochem. J.* **1993**, *293*, 781-788.

[6] Chiba, S.; Hiromi, K.; Minamiura, N.; Ohnishi, M.; Shimomura, T.; Suga, K.; Suganuma, T.; Tanaka, A.; Tomioka, S.; Yamamoto, T. Quantitative study on anomeric forms of glucose produced by α-glucosidases. *J. Biochem.* **1979**, *85*, 1135-1141.

[7] Chiba, S.; Kimura, A.; Matsui, H. Quantitative study of anomeric forms of glucose produced by α-glucosidases and glucoamylases. *Agric. Biol. Chem.* **1983**, *47*, 1741-1746.

[8] Palcic, M. M.; Scaman, C. H.; Otter, A.; Szpacenko, A.; Romaniouk, A.; Li, Y. X.; Vijay, I. K. Processing α-glucosidase I is an inverting glycosidase. *Glycoconj. J.* **1999**, *16*, 351-355.

[9] Hanozet, G.; Pircher, H.P.; Vanni, P.; Oesch, B.; Semenza, G. An example of enzyme hysteresis. The slow and tight interaction of some fully competitive inhibitors with small intestinal sucrase. *J. Biol. Chem.* **1981**, *256*, 3703-3711.

[10] Zitzmann, N.; Mehta, A. S.; Carrouée, S.; Butters, T. D.; Platt, F. M.; McCauley, J.; Blumberg, B. S.; Dwek, R. A.; Block, T. M. Imino sugars inhibit the formation and secretion of bovine viral diarrhea virus, a pestivirus model of hepatitis C virus: Implications for the development of broad spectrum anti-hepatitis virus agents. *Proc. Natl. Acad. Sci. USA* **1999**, *96*, 11878-11882.

[11] Seiichiro Ogawa, S.; Ashiura, M.; Uchida, C. Synthesis of α-glucosidase inhibitors: kojibiose-type pseudodisaccharides and a related pseudotrisaccharide. *Carbohydr. Res.* **1998**, *307*, 83-95.

[12] Nishio. T.; Miyake. Y.; Tsujii. H.; Hakamata. W.; Kadokura. K.; Oku. T. Hydrolytic activity of α-mannosidase against deoxy derivatives of *p*-nitrophenyl α-D-mannopyranoside. *Biosci. Biotech. Biochem.* **1996**, *60*, 2038-2042.

[13] Hakamata. W.; Nishio. T.; Oku. T. Synthesis of *p*-nitrophenyl 3- and 6-deoxy-α-D-glucopyranosides and their specificity to rice α-glucosidase. *J. Appl. Glycosci.* **1999**, *46*, 459-463.

[14] Hakamata, W.; Nishio, T.; Oku, T. Hydrolytic activity of α-galactosidase against deoxy derivatives of *p*-nitrophenyl α-D-galactopyranoside. *Carbohydr. Res.* **2000**, *324*, 107-115.

[15] Hakamata, W.; Nishio, T.; Sato, R.; Mochizuki, T.; Tsuchiya, K.; Yasuda, M.; Oku, T. Synthesis of monomethyl derivatives of *p*-nitrophenyl α-D-gluco, galacto, and mannopyranosides and their hydrolytic properties against α-glycosidase. *J. Carbohydr. Chem.* **2000**, *19*, 359-377.

[16] Nishio, T.; Hakamata, W.; Kimura, A.; Chiba, S.; Takatsuki, A.; Kawachi, R.; Oku, T. Glycon specificity profiling of α-glucosidases using monodeoxy and mono-*O*-methyl derivatives of *p*-nitrophenyl α-D-glucopyranoside. *carbohydr. Res.* **2003**, *337*, 629-634.

[17] Hakamata, W.; Muroi, M.; Nishio, T.; Oku, T.; Takatsuki, A. Recognition properties of processing α-glucosidase I and α-glucosidase II. *J. Carbohydr. Chem.* **2004**, *23*, 27-39.

[18] Nishio, T.; Hakamata, W.; Ogawa, M.; Nakajima, K.; Matsuishi, Y.; Kawachi, R.; Oku, T. Investigations of useful α-glycosidase for the enzymatic synthesis of rare sugar oligosaccharides. *J. Appl. Glycosci.* **2005**, *52*, 153-160.

[19] Hakamata, W.; Muroi, M.; Kadokura, K.; Nishio, T.; Oku, T.; Kimura, A.; Chiba, S.; Takatsuki, A. Aglycon Specificity Profiling of α-Glucosidases Using Synthetic probes. *Bioorg. Med. Chem. Lett.* **2005**, *15*, 1489-1492.

[20] Hakamata, W.; Muroi, M.; Nishio, T.; Oku, T.; Takatsuki, A.; Osada, H.; Fukuhara, K.; Okuda, H.; Kurihara, M. *N*-Linked Oligosaccharide Processing Enzymes as Molecular Targets for Drug Discovery. *J. Appl. Glycosci.* **2006**, *53*, 149-154.

[21] Hakamata W. Yamamoto E.; Muroi M.; Mochizuki T.; Kurihara M.; Okuda H.; Fukuhara, K. Design and Synthesis of α-glucosidase inhibitor having DNA cleaving activity. *J. Appl. Glycosci.* **2006**, *53*, 255-260.

[22] Caspary, W. F.; Graf, S. Inhibition of human intestinal α-glucosidehydrolases by a new complex oligosaccharide. *Res. Exp. Med.* **1979**, *175*, 1-6.

[23] Kornfeld, R.; Kornfeld, S. Assembly of asparagine-linked oligosaccharides. *Annu. Rev. Biochem.* **1985**, *54*, 631-664.

[24] Killilea, T. Long-term consequences of type 2 diabetes mellitus: economic impact on society and managed care. *Am. J. Manag. Care* **2002**, *8*, S441-S449.

[25] Mitra, N.; Sinha, S.; Ramya, T. N.; Surolia, A. *N*-linked oligosaccharides as outfitters for glycoprotein folding, form and function. *Trends. Biochem. Sci.* **2006**, *31*, 156-163.

[26] Bukau, B.; Weissman Horwich, A. Molecular chaperones and protein quality control. *Cell* **2006**, *125*, 443-451.

[27] Hanefeld, M.; Fischer, S.; Schulze, J.; Spengler, M.; Wargenau, M.; Schollberg, K.; Fücker, K. Therapeutic potentials of acarbose as first-line drug in NIDDM insufficiently treated with diet alone. *Diabetes Care*. **1991**, *14*, 732-737.

[28] Helenius, A.; Aebi, M. Roles of *N*-linked glycans in the endoplasmic reticulum. *Annu. Rev. Biochem.* **2004**, *73*, 1019-1049.

[29] Ellgaard, L.; Helenius, A. Quality control in the endoplasmic reticulum. *Nat. Rev. Mol. Cell Biol.* **2003**, *4*, 181-91.

[30] Helenius, A.; Aebi, M. Intracellular functions of *N*-linked glycans. *Science* **2001**, *291*, 2364-2369.

[31] Ellgaard, L.; Molinari, M.; Helenius, A. Setting the standards: Quality control in the secretory pathway. *Science* **1999**, *286*, 1882-1888.

[32] Suzuki, T.; Funakoshi, Y. Free *N*-linked oligosaccharide Chains: Formation and degradation. *Glycoconj. J.* **2006**, *23*, 291-302.

[33] Meusser, B.; Hirsch, C.; Jarosch, E.; Sommer, T. ERAD: The long road to destruction. *Nat. Cell Biol.* **2005**, *7*, 766-772.

[34] Lord, J.; Roberts, L.; Stirling, C. Quality control: Another player joins the ERAD cast. *Curr. Biol.* **2005**, *15*, R963-R964.

[35] Yoshida, Y. A novel role for *N*-glycans in the ERAD system. *J. Biochem.* **2003**, *134*, 183-190.

[36] Ma, Y.; Hendershot, L. M. The unfolding tale of the unfolded protein response. *Cell* **2001**, *107*, 827-830.

[37] Schroder, M.; Kaufman, R. J. ER stress and the unfolded protein response. *Mutat. Res.* **2005**, *569*, 29-63.

[38] Fiaux, H.; Popowycz, F.; Favre, S.; Schütz, C.; Vogel, P.; Gerber-Lemaire, S. Juillerat-Jeanneret, L. Functionalized pyrrolidines inhibit α-mannosidase activity and growth of human glioblastoma and melanoma cells. *J. Med. Chem.* **2005**, *48*, 4237-4246.

[39] Van Den Elsen, J. M.; Kuntz, D. A.; Rose, D. R. Structure of golgi α-mannosidase II: A target for inhibition of growth and metastasis of cancer cells. *EMBO J.* **2001**, *20*, 3008-3017.

[40] Dennis, J. M.; Granovsky, M.; Warren, C. E. Protein glycosylation in development and disease. *Bioassays* **1999**, *21*, 412-421.

[41] Granovskya, M.; Warrena, C. E. Glycoprotein glycosylation and cancer progression. *Biochim. Biophys. Acta* **1999**, *1473*, 21-34.

[42] Pili, R.; Chang, J.; Partis, R. A.; Mueller, R. A.; Chrest, F. J.; Passaniti, A. The α-glucosidase I inhibitor castanospermine alters endothelial cell glycosylation, prevents angiogenesis, and inhibits tumor growth. *Cancer Res.* **1995**, *55*, 2920-2926.

[43] Goss, P. E.; Baker, M. A.; Carver, J. P.; Dennis, J. W. Inhibitors of carbohydrate processing: A new class of anticancer agents. *Clin. Cancer Res.* **1995**, *1*, 935-944.

[44] Atsumi, S.; Nosaka, C.; Ochi, Y.; Iinuma, H.; Umezawa, K. Inhibition of experimental metastasis by an α-glucosidase inhibitor, 1,6-Epi-cyclophellitol. *Cancer Res.* **1993**, *53*, 4896-4899.

[45] De Clercq, E. Antiviral therapy for human immunodeficiency virus infections. *Clin. Microbiol. Rev.* **1995**, *8*, 200-239.

[46] Robina, I.; Moreno-Vargas, A. J.; Carmona, A. T.; Vogel, P. Glycosidase inhibitors as potential HIV entry inhibitors? *Curr. Drug Metab.* **2004**, *5*, 329-361.

[47] Naoki, A. Glycosidase inhibitors: Update and perspectives on practical use. *Glycobiol.* **2003**, *13*, 93R-104R.

[48] Chapel, C.; Garcia, C.; Roingeard, P.; Zitzmann, N.; Dubuisson, J.; A. Dwek, R.: Trépo, C.; Zoulim, F.; Durantel, D. Antiviral effect of α-glucosidase inhibitors on viral morphogenesis and binding properties of hepatitis C virus-like particles. *J. Gen. Virol.* **2006**, *87*, 861-871.

[49] Tong, S. Mechanism of HBV genome variability and replication of HBV mutants. *J. Clin. Virol.* **2005**, *34*, S134-138.

[50] Saito, T.; Yamaguchi, I. Effect of glycosylation and glucose trimming inhibitors on the influenza a virus glycoproteins. *J. Vet. Med. Sci.* **2000**, *62*, 575-581.

[51] Oostra, M.; de Haan, C. A. M.; de Groot, R. J.; Rottier, P. J. M. Glycosylation of the severe acute respiratory syndrome coronavirus triple-spanning membrane proteins 3a and M. *J. Virol.* **2006**, *80*, 2326-2336.

[52] Liang, P. H.; Cheng, W. C.; Lee, Y. L.; Yu, H. P.; Wu, Y.T.; Lin, Y. L.; Wong, C. H. Novel five-membered iminocyclitol derivatives as selective and potent glycosidase inhibitors: New structures for antivirals and osteoarthritis. *Chembiochem.* **2006**, *7*, 165-73.

[53] De Clercq, E. Highlights in the development of new antiviral agents. *Mini. Rev. Med. Chem.* **2002**, *2*, 163-175.

[54] Fesik, S. W. Promoting apoptosis as a strategy for cancer drug discovery. *Nat. Rev. Cancer* **2005**, *5*, 876-885.

[55] Fischer, U.; Schulze-Osthoff, K. Apoptosis-based therapies and drug targets. *Cell Death Differ.* **2005**, *12*, 942-961.

[56] Yoshida, Y.; Chiba, T.; Tokunaga, F.; Kawasaki, H.; Iwai, K.; Suzuki, T.; Ito, Y.; Matsuoka, K.; Yoshida, M.; Tanaka, K.; Tai, T. E3 ubiquitin ligase that recognizes sugar chains. *Nature* **2002**, *418*, 438-442.

[57] Lew, W.; Chen, X.; Kim, C.U. Discovery and development of GS 4104 (oseltamivir) an orally active influenza neuraminidase inhibitor. *Curr. Med. Chem.* **2000**, *7*, 663-672.

[58] Dwek, R. A.; Butters, T. D.; Platt, F. M.; Zitzmann, N. Targeting glycosylation as a therapeutic approach. *Nat. Rev. Drug Discov.* **2002**, *1*, 65-75.

[59] Bertozzi, C. R.; Kiessling, L. L. Chemical glycobiology. *Science* **2001**, *291*, 2357-2364.

[60] Inouye, S.; Tsuruoka, T.; Nida, T. The structure of nojirimycin, a piperidinose sugar antibiotic. *J. Antibiot.* **1966**, *19*, 288-92.

[61] Ishida, N.; Kumagai, K.; Niida, T.; Hamamoto, K.; Shomura, T. Nojirimycin, a new antibiotic. I. Taxonomy and fermentation. *J. Antibiot.* **1967**, *20*, 62-65.

[62] Ishida, N.; Kumagai, K.; Niida, T.; Tsuroka, T.; Yumoto, H. Nojirimycin, a new antibiotic. II. Isolation, characterization and biological activity. *J. Antibiot.* **1967**, *20*, 66-71.

[63] Inouye, S.; Tsuruoka, T.; Ito, T.; Niida, T. Structure and synthesis of nojirimycin. *Tetrahedron* **1968**, *24*, 2125-2144.

[64] Legler, G. Glycoside hydrolases: Mechanistic information from studies with reversible and irreversible inhibitors. *Adv. Carbohydr. Chem. Biochem.* **1990**, *48*, 319-384.

[65] Heightman, T. D.; Vasella, A. T. Recent insights into inhibition, structure, and mechanism of configuration-retaining glycosidases. *Angew. Chem. Int. Ed.* **1999**, *38*, 750-770.

[66] Ganem, B. Inhibitors of carbohydrate-processing enzymes: Design and synthesis of sugar-shaped heterocycles. *Acc. Chem. Res.* **1996**, *29*, 340-370.

[67] El Ashry, E. S. H.; Rashed, N.; Shobier, A. H. S. α-Glycosidase inhibitors and their chemotherapeutic value, Part 1. *Pharamazie* **2000**, *55*, 251-262.

[68] El Ashry, E. S. H.; Rashed, N.; Shobier, A. H. S. α-Glycosidase inhibitors and their chemotherapeutic value, Part 2. *Pharamazie* **2000**, *55*, 331-348.

[69] El Ashry, E. S. H.; Rashed, N.; Shobier, A. H. S. α-Glycosidase inhibitors and their chemotherapeutic value, Part 3. *Pharamazie* **2000**, *55*, 403-415.

[70] Zechel, D. L.; Withers, S. G. Glycosidase mechanisms: Anatomy of a finely tuned catalyst. *Acc. Chem. Res.* **2000**, *33*, 11-18.

[71] Asano, N.; Nash, R. J.; Molyneux, R. J.; Fleet, G. W. J. Sugar-mimic glycosidase inhibitors: Natural occurrence, biological activity and prospects for therapeutic application. *Tetrahedron Asymmetry* **2000**, *11*, 1645-1680.

[72] Butters, T. D.; Dwek, R. A.; Platt, F. M. *Chem. Rev.* **2000**, *100*, 4683-4696.

[73] Watson, A. A.; Fleet, G. W. J.; Asano, N.; Molyneux, R. J.; Nash, R. J. *Phytochemistry* **2001**, *56*, 265-295.

[74] Nakao, Y.; Maki, T.; Matsunaga, S.; van Soest, R. W. M.; Fusetani, N. Penarolide sulfates A1 and A2, new α-glucosidase inhibitors from a marine sponge penares sp. *Tetrahedron* **2000**, *56*, 8977-8987.

[75] Sou, S.; Mayumi, S.; Takahashi, H.; Yamasaki, R.; Kadoya, S.; Sodeoka, M.; Hashimoto, Y. Novel α-glucosidase inhibitors with a Tetrachlorophthalimide Skeleton. *Bioorg. Med. Chem. Lett.* **2000**, *10*, 1081-1084.

[76] Hakamata, W.; Nakanishi, I.; Masuda, Y.; Shimizu, T.; Higuchi, H.; Nakamura, Y.; Saito, S.; Urano, S.; Oku, T.; Ozawa, T.; Ikota, N.; Miyata, N.; Okuda, H.; Fukuhara, K. Planar catechin analogues with alkyl side chains: A potent antioxidant and an α-glucosidase inhibitor. *J. Am. Chem. Soc.* **2006**, *128*, 6524-6525.

[77] Kundu, B.; Rastogi, S.K.; Ahmad, R.; Srivastava, A.K. Identification of novel α-glucosidase inhibitors by screening libraries based on *N*-[4-(benzyloxy) benzoyl] alanine derivatives. *Comb. Chem. High Throughput Screen* **2002**, *5*, 545-550.

[78] Zheng, W.; Padia, J.; Urban, D.J.; Jadhav, A.; Goker-Alpan, O.; Simeonov, A.; Goldin, E.; Auld, D.; LaMarca, M.E.; Inglese, J.; Austin, C.P.; Sidransky, E. Three classes of glucocerebrosidase inhibitors identified by quantitative high-throughput screening are chaperone leads for Gaucher disease. *Proc. Natl. Acad. Sci. USA* **2007**, *104*, 13192-13197.

[79] Tarling, C.A.; Woods, K.; Brastianos, H.C.; Zhang, R.; Brayer, G.D.; Andersen, R.J.; Withers, S.G. The search for novel human pancreatic α-amylase inhibitors: high-throughput screening of terrestrial and marine natural product extracts. *ChemBiochem* **2008**, *9*, 433-438.

[80] Chiba, S. α-Glucosidase. In *Handbook of Amylases & Related Enzymes*; The Amylase Research Society of Japan; Eds.; Pergamon Press: Oxford, 1988; pp 104-116.

[81] Chiba, S. Molecular mechanism in α-glucosidase and glucoamylase. *Biosci. Biotechnol. Biochem.* **1997**, *61*, 1233-1239.

[82] Bause, E.; Schweden, J.; Gross, A.; Orthen, B. Purification and characterization of trimming glucosidase I from pig liver. *Eur. J. Biochem.* **1989**, *183*, 661-669.

[83] Shailubhai, K.; Pratta, M. A.; Vijay, I. K. Purification and characterization of glucosidase I involved in *N*-linked glycoprotein processing in bovine mammary gland. *Biochem. J.* **1987**, *247*, 555-562.

[84] Burns, D. M.; Touster, O. Purification and characterization of glucosidase II, an endoplasmic reticulum hydrolase involved in glycoprotein biosynthesis. *J. Biol. Chem.* **1982**, *257*, 9991-10000.

[85] Frandsen, T. P.; Svensson, B. Plant α-glucosidase of the glycoside hydrolase family 31. Molecular properties, substrate specificity, reaction mechanism, and comparison with family members of different origin. *Plant Mol. Biol.* **1998**, *37*, 1-13.

[86] Hino, Y.; Rothman, J. E. Glucosidase II, a glycoprotein of the endoplasmic reticulum membrane. Proteolytic cleavage into enzymatically active fragments. *Biochemistry* **1985**, *24*, 800-805.

[87] Frandsen, T. P.; Lok, F.; Mirgorodskaya, E.; Roepstorff, P.; Svensson, B. Purification, enzymatic characterization, and nucleotide sequence of a high-isoelectric-point α-glucosidase from barley malt. *Plant Physiol.* **2000**, *123*, 275-286.

[88] Kita, A.; Matsui, H.; Somoto, A.; Kimura, A.; Takata, M.; Chiba, S. Substrate specificity and subsite affinities of crystalline α-glucosidase from *Aspergillus niger*. *Agric. Biol Chem.* **1991**, *55*, 2327-2335.

[89] Shailubhai, K.; Pratta, M. A.; Vijay, I. K. Purification and characterization of glucosidase I involved in *N*-linked glycoprotein processing in bovine mammary gland. *Biochem. J.* **1987**, *247*, 555-562.

[90] Kaushal, G. P.; Elbein, A. D. Glycosidase inhibitor in study of glycoconjugates. *Meth. Enzymol.* **1994**, *230*, 316-329.

[91] Tsujii, E.; Muroi, M.; Shiragami, N.; Takatsuki, A. Nectrisine is a potent inhibitor of α-glucosidases, demonstrating activities similarly at enzyme and cellular levels. *Biophys. Biophys. Res. Commun.* **1996**, *220*, 459-466.

[92] Bajorath, J. Integration of virtual and high-throughput screening. *Nat. Rev. Drug Discov.* **2002**, *1*, 882-894.

[93] Steven, P.; David, J. E.; Remy, H. Challenges of target/compound data integration from disease to chemistry: A case study of dihydrofolate reductase inhibitors. *Curr. Drug Discov. Technol.* **2005**, *2*, 75-87.

[94] Martin, S. Current status of virtual screening as analyzed by target class. *J. Med. Chem.* **2006**, *2*, 89-112.

[95] Ernsta, H. A.; Leggioa, L. L.; Willemoësa, M.; Leonarde, G.; Blumd, P.; Larsena, S. Sructure of the *Sulfolobus solfataricus* α-glucosidase: Implications for domain conservation and substrate recognition in GH31. *J. Mol. Biol.* **2006**, *358*, 1106-1124.

[96] Lovering, A.L.; Lee, S.S.; Kim, Y.W.; Withers, S.G.; Strynadka, N.C. Mechanistic and structural analysis of a family 31 α-glycosidase and Its glycosyl-enzyme intermediate *J. Biol. Chem.* **2005**, *280*, 2105-2115.

[97] PDB ID: 1WE5, Crystal structure of α-xylosidase from *Escherichia coli*, To be published.

[98] Kim, Y.-W.; Lovering, A. L.; Chen, H.; Kantner, T.; McIntosh, L. P.; Strynadka, N. C. J.; Withers, S. G. Expanding the thioglycoligase strategy to the synthesis of α-linked thioglycosides allows structural investigation of the parent enzyme/substrate complex. *J. Am. Chem. Soc.* **2006**, *128*, 2202-2203.

[99] Okuyama, M.; Kaneko, A.; Mori, H.; Chiba, S.; Kimura, A. Structural elements to convert *Escherichia coli* α-xylosidase (YicI) into α-glucosidase. *FEBS Lett.* **2006**, *580*, 2707-2711.

[100] Okuyama, M.; Kang, M.; Yaoi, K.; Mitsuishi, Y.; Mori, H.; Kimura, A. Substrate recognition of *Escherichia coli* YicI (α-xylosidase). *J. Appl. Glycosci.* **2008**, *55*, 111-118.

[101] Watanabe, K.; Hata, Y.; Kizaki, H.; Katsube, Y.; Suzuki, Y. The refined crystal structure of *Bacillus cereus* Oligo-1,6-glucosidase at 2.0 Å resolution: Structural characterization of proline-substitution sites for protein thermostabilization. *J. Mol. Biol.* **1997**, *269*, 142-153.

[102] MOE software available from Chemical Computing Inc., Montreal Canada. Consult http://www.chemcomp.com for further information.

[103] von Itzstein, M.; Wu, W.-Y.; Kok, G. B.; Pegg, M. S.; Dyason, J. C.; Jin, B.; Van Phan, T.; Smythe, M. L.; White, H. F.; Oliver, S. W.; Colman, P. M.; Varghese, J. N.; Ryan, D. M.; Woods, J. M.; Bethell, R. C.; Hotham, V. J.; Cameron, J. M.; Penn, C. R. Rational design of potent sialidase-based inhibitors of influenza virus replication. *Nature* **1993**, *363*, 418-423.

[104] Itzstein, M.; Wu, W.-Y.; Jina, B. The Synthesis of 2,3-Didehydro-2,4-dideoxy-4-guanidinyl-*N*-acetylneuraminic acid: A potent influenza virus sialidase inhibitor. *Carbohydr. Res.* **1994**, *259*, 301-305.

[105] Alymova, I. V.; Taylor, G. Portner, A neuraminidase inhibitors as antiviral agents. *Curr. Drug Targets-Infect. Disord.* **2005**, *5*, 401-409.

[106] Mann, M. C.; Islam, T.; Dyason, J. C.; Florio, P.; Trower, C. J.; Thomson, R. J.; Itzstein, M. Unsaturated *N*-acetyl-D-glucosaminuronic acid glycosides as inhibitors of influenza virus sialidase. *Glycoconj. J.* **2006**, *23*, 127-133.

[107] Wei, D. Q.; Du, Q. S.; Sun, H.; Chou, K. C. Insights from Modeling the 3D Structure of H5N1 Influenza Virus Neuraminidase and Its Binding Interactions with Ligands. *Biochem. Biophys. Res. Commun.* **2006**, *344*, 1048-1055.

[108] Park, H.; Hwang, K.Y.; Oh, K.H.; Kim, Y.H.; Lee, J.Y.; Kim, K. Discovery of novel α-glucosidase inhibitors based on the virtual screening with the homology-modeled protein structure. *Bioorg. Med. Chem. Lett.* **2008**, *16*, 284-292.

[109] Park, H.; Hwang, K. Y.; Kim, Y.H.; Oh, K.H.; Lee, J.Y.; Kim, K. Discovery and biological evaluation of novel α-glucosidase inhibitors with *in vivo* antidiabetic effect. *Bioorg. Med. Chem. Lett.* **2008**, *18*, 3711-3715.

[110] Bharatham, K.; Bharatham, N.; Park, K.H.; Lee, K.W. Binding mode analyses and pharmacophore model development for sulfonamide chalcone derivatives, a new class of α-glucosidase inhibitors. *J. Mol. Graph Model.* **2008**, *26*, 1202-1212.

[111] Molegro software available from BiRC - Bioinformatics Research Center, Denmark. Consult http://www.molegro.com/ for further information.

[112] Accelrys Discovery Studio available from Accelrys, Inc., San Diego, CA, USA. Consult http://www. accelrys.com/ for further information.

Biosci. Biotechnol. Biochem., **73** (1), 189–191, 2009

Note

Crystallization and Structural Analysis of Cytochrome c_6 from the Diatom *Phaeodactylum tricornutum* at 1.5 Å Resolution

Hideharu AKAZAKI,[1] Fumihiro KAWAI,[2] Masaki HOSOKAWA,[1] Toshiyuki HAMA,[1] Hirotaka CHIDA,[1] Takako HIRANO,[1] Boon-Keng LIM,[3] Nobuo SAKURAI,[3] Wataru HAKAMATA,[1] Sam-Yong PARK,[2] Toshiyuki NISHIO,[1] and Tadatake OKU[1,†]

[1]*Bio-Organic Chemistry Laboratory, Graduate School of Bioresource Sciences, Nihon University, 1866 Kameino, Fujisawa-shi, Kanagawa 252-8510, Japan*
[2]*Protein Design Laboratory, Graduate School of Integrated Science, Yokohama City University, 1-7-29 Suehiro-cho, Tsurumi, Yokohama 230-0045, Japan*
[3]*Kajima Corporation, Kajima Technical Research Institute, Environmental Engineering and Bioengineering Group-Hayama, 2400 Isshiki, Hayama-cho, Miura-gun, Kanagawa 240-0111, Japan*

Received July 8, 2008; Accepted October 8, 2008; Online Publication, January 7, 2009
[doi:10.1271/bbb.80472]

We determined for the first time the crystal structure of diatom cytochrome c_6 from *Phaeodactylum tricornutum* at 1.5 Å resolution. The overall structure of the protein was classified as a class I *c*-type cytochrome. The physicochemical properties of the protein were examined by denaturation with guanidine hydrochloride and urea, and compared with those of other algal cytochrome c_6.

Key words: cytochrome c_6; crystal structure; diatom; physicochemical property; structural stability

It is thought that diatoms acquired their chloroplasts and photosynthetic proteins *via* secondary endosymbiosis involving a primitive red algal endosymbiont and a non-photosynthetic eukaryote host.[1,2] The chlorophylls and photosynthetic electron carriers are different among cyanobacteria, diatoms, and green, red, and brown algae. In the case of green algae that contain chlorophyll *b* and cyanobacteria, a heme-Fe protein cytochrome (cyt) c_6 and a copper protein plastocyanin (PC) function as electron carriers between cyt *f*, which is part of the membrane-embedded cytochrome b_6f complex, and the P700 reaction center of photosystem I. It is widely believed that PC is not present in chlorophyll-*b*-non-containing algae such as red, and brown algae and diatoms, and that only cyt c_6 acts as an electron carrier in these organisms. But recent study has shown for the first time that a marine diatom, *Thalassiosira oceanica*, contains a PC.[3] To date, diatom PC has been confirmed only in marine diatom *T. oceanica*, and the closely related coastal species *Thalassiosira weissflogii* does not contain this copper protein.

Cyt c_6 is a high-potential, soluble, low-spin heme protein. Although the physicochemical properties and cDNA sequence of the protein from the diatom *Phaeodactylum tricornutum* have been examined,[4,5] the tertiary structure of diatom cyt c_6 remains unresolved. In this study, we determined the crystal structure and physicochemical properties of diatom cyt c_6, and compared them with those of other algal and cyanobacterial cyts c_6.

P. tricornutum (UTEX no. 646) was grown at 20 °C for 8 d under a 12 h light/12 h dark cycle at 60 $\mu E\,m^{-2}\,S^{-1}$ with fluorescent lamps in PES medium supplemented with 100 mg/l of $NaNO_3$, 0.1 mg/l of thiamine HCl, 1.0 µg/l of vitamin B_{12}, 7.0 mg/l of $Fe(NH_4)_2 \cdot 6H_2O$, 2.0 mg/l of H_2BO_3, 3.0 mg/l of Na_2-EDTA, 0.4 mg/l of $MnCl_2$, 0.01 mg/l of $CaCl_2$, 40 µg/l of $ZnCl_2$, 0.1 mg/l of $FeCl_2$, and 90 mg/l of $Na_2SiO_3 \cdot 9H_2O$. cDNA cloning of *P. tricornutum* cyt c_6 (Ptc6) was carried out by previous methods.[5] The mature Ptc6 sequence was amplified using a forward primer (5′-AGCCATGGGGGACGTCGGTGCTGGTG-AGC-3′), corresponding to the codons for the amino acid residues of the cyt c_6 N-terminal region, and a reverse primer (5′-GCGGATCCTTACTCCCATCCGG-CTTCAGCG-3′), corresponding to the codons for the amino acid residues of the C-terminal region. Vector construction, overproduction in *Escherichia coli*, and purification of recombinant Ptc6 were performed as described methods.[6] The degree of purity was confirmed by tricine sodium dodecyl sulfate-polyacrylamide gel electrophoresis.

The UV/visible spectra and redox titration of the purified recombinant Ptc6 were measured according to previous methods.[7] The UV/vis absorption spectra of reduced and oxidized Ptc6 are shown in Fig. 1A. In the reduced form, the α-, β-, γ (soret)-, and δ-absorption maxima peaks appeared at 553.0 nm, 523.0 nm, 417.0 nm, and 316.0 nm, respectively. For the oxidized form of recombinant Ptc6, the absorption maxima peaks of $\alpha + \beta$, γ (soret), and δ were 528.5 nm, 411.5 nm, and 360.0 nm respectively, and a shoulder peak at 695.0 nm, indicating a His-Fe-Met coordination, was observed (Fig. 1A, inset). The UV/vis absorption spectra of recombinant Ptc6 were similar to the previous results.[4] The redox data were analyzed with a theoretical curve based on the Nernst equation ($n = 1$): $E = E^0 + (RT/nF)\ln([cyt_{oxi}]/[cyt_{red}])$. In good agreement with a previously published report,[4] the redox potential of this protein was +349 mV (Fig. 1B).

Denaturation of oxidized Ptc6 and oxidized *Porphyra yezoensis* cyt c_6 with guanidine hydrochloride (Gdn-

† To whom correspondence should be addressed. Tel/Fax: +81-466-84-3950; E-mail: oku@brs.nihon-u.ac.jp

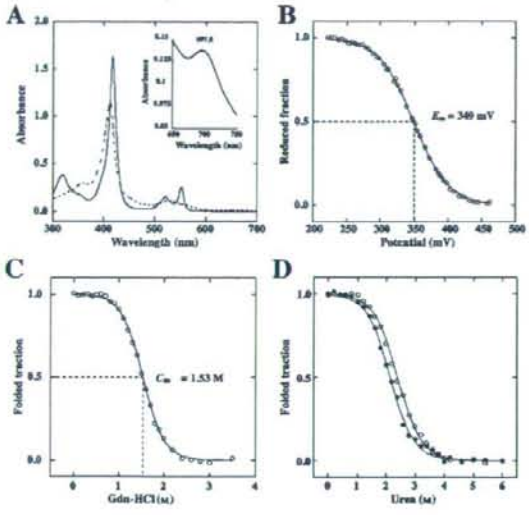

Fig. 1. Physicochemical Properties of Diatom Ptc6.

A, UV/visible spectra of reduced (solid line) and oxidized (broken line) forms of Ptc6. Absorption spectra of 10 μM Ptc6 were measured in 10 mM sodium phosphate (pH 7.0) at 25 °C. The inset shows the 700 nm band of the oxidant form at 80 μM. Sodium dithionite and potassium ferricyanide were used as oxidant and reductant respectively. B, Redox titration of Ptc6. The redox state of the protein was determined by changing the α-band absorption spectrum using a Hitachi U-3310 spectrophotometer. The smooth curve was drawn by the Nernst equation giving the best fit to the data using a Sigma Plot program. C, Gdn-HCl denaturation curves of oxidized Ptc6. Ptc6 was denatured by titration with Gdn-HCl in 10 mM sodium phosphate (pH 7.0) at a protein concentration of 5 μM. D, Urea denaturation curves of oxidized Ptc6 and red algal cyts c_6. Ptc6 and red algal cyts c_6 were denatured by titration with urea in 10 mM sodium phosphate (pH 7.0) at a protein concentration of 5 μM. Ptc6 (circles); red algal cyt c_6 (closed circles).

HCl) and urea as denaturants was measured following previous reports.[7,8] Purification of the red alga *P. yezoensis* cyt c_6 was performed as previously described.[7] The denaturation data were analyzed with a theoretical curve based on $\Delta G_{unf} = -RT \ln K_D = \Delta G^0{}_{unf} - m$[denaturant] by assuming the two-state folding-unfolding transition with the equilibrium constant K_D. The thermodynamic parameter, $\Delta G^0{}_{unf}$, shows the free energy change from the folded state to the unfolded state in the absence of a denaturant, and m shows the dependence of the free energy change ($\Delta G^0{}_{unf}$) on the denaturant concentration. In the case of Gdn-HCl as denaturant, the C_m, $\Delta G^0{}_{unf}$, and m values of the oxidized Ptc6 were 1.53 M, 3.83 kcal/mol, and 2.50 kcal/mol/M respectively (Fig. 1C). The values for Ptc6 were higher than those for the red alga *P. yezoensis* cyt c_6 ($C_m = 0.95$ M, $\Delta G^0{}_{unf} = 2.43$ kcal/mol, $m = 2.56$ kcal/mol/M).[7] In the case of urea, the values for oxidized Ptc6 were 2.39 M, 3.73 kcal/mol, and 1.56 kcal/mol/M respectively. The values for Ptc6 were also higher than those for the red alga *P. yezoensis* cyt c_6 ($C_m = 2.22$ M, $\Delta G^0{}_{unf} = 2.87$ kcal/mol, $m = 1.29$ kcal/mol/M) (Fig. 1D). These results indicate that the structural stability of Ptc6 is higher than that of red algal cyt c_6. The soret peaks for Ptc6 were blue-shifted by urea (from 411.5 nm to 404.5 nm) and Gdn-HCl (from 411.5 nm to 406.5 nm) denaturation. These blue-shifts of the soret peak are indicative of conversion of the heme toward a high-spin form with disruption of heme six coordinated.[9] The soret peaks of the unfolded state of Ptc6 were red-shifted by dialysis against 10 mM sodium phosphate buffer (pH 7.0), and the soret peaks of refolded state of Ptc6 agreed with those of native Ptc6. Thus these results suggest that urea and Gdn-HCl denaturation of Ptc6 are reversible.

Table 1. Crystal Parameters, Data Collection, and Structure Refinement

Data-collection statistics	
Temperature (K)	100
Resolution range (Å)	50.0–1.50
Space group	*I*23
Unit cell parameters (Å)	$a = b = c = 80.380$
Reflections (Measured/Unique)	273393/13706
Completeness (Overall/Outer Shell, %)	97.8/100
R_{merge} (Overall/Outer Shell, %)	4.1/6.4
Redundancy (Overall/Outer Shell)	20.0
Mean [I/s (I)]	32.7
Refinement statistics	
Resolution range (Å)	20.0–1.50
cut-off/reflections used	0.0/13675
R factor/R-free (%)	16.4/20.2%
R.m.s.d. bond length/bond angle (°)	0.009/1.148
Residues in most favourable region (%)	86.1%
Residues in additional allowed region (%)	12.5%
Residues of disallowed region (%)	1.5%

$R_{merge} = \sum |I_i - \langle I \rangle| / \sum I_i$, where I_i is the intensity of an observation and $\langle I \rangle$ is the mean value for its unique reflection; summations are overall reflections. R factor $= \sum_h |F_o(h) - F_c(h)| / \sum hF_o(h)$, where F_o and F_c are the observed and calculated structure-factor amplitudes respectively. The free R factor was calculated with 5% of the data excluded from the refinement. Values in parentheses are for the outer shell, with a resolution within 50.0–1.50 Å.

For crystallization of Ptc6, the purified recombinant protein was dissolved in super-pure water to prepare a concentrated protein solution of 50 mg ml^{-1}. Ptc6 was crystallized by vapor diffusion; the hanging drops used contained a 1:1 mixture of protein and reservoir solution. Cyt c_6 was allowed to crystallize over a reservoir containing 0.1 M Tris–HCl pH 8.5, 0.2 M $MgSO_4$, and 35% Polyethylene Glycol 4000. X-ray diffraction data were collected on the BL-5A (Photon Factory, Tsukuba, Japan). The data set was processed with HKL2000 and scaled with SCALE-PACK.[10] The structure of Ptc6 was determined by molecular replacement using the program MOLREP[11] and the structure of *P. yezoensis* cyt c_6.[12] The structure of Ptc6 was refined with Refmac in the CCP4 program suite. Water molecules were added using a water pick script of CNS, and refinement was continued using REFMAC5.[11] The final model obtained had an R-factor of 16.4% and a free R-factor of 20.2%. Manual model building was carried out using Coot.[13] Solvent molecules were placed at positions where spherical electron density peaks were found above 1.5σ in the $|2F_o - F_c|$ map and above 3.0σ in the $|F_o - F_c|$ map, and where stereochemically reasonable hydrogen bonds were allowed. A summary of data collection and refinement statistics is given in Table 1. The refined crystallographic coordinates and structure factor amplitudes have been deposited in the Protein Data Bank (PDB entry 3dmi).

The first crystal structure of diatom cyt c_6 was determined at 1.5 Å resolution. The crystal belonged to space group I_{23}, with unit cell parameters $a = b = c = 80.38$ Å and one molecule per asymmetric unit. The overall structure of Ptc6 followed the topology of class I c-type cyts (Fig. 2B). An amino acid sequence comparison of diatom Ptc6 with *Chlamydomonas reinhardtii*,

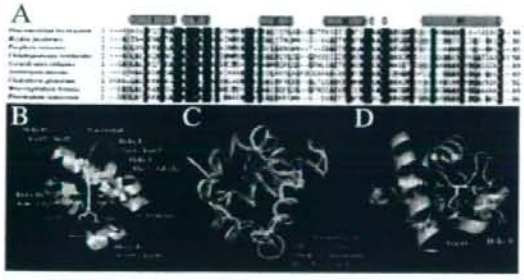

Fig. 2. Aligned Amino Acid Sequences of Cyts c_6 with Reported Crystal Structure and Crystal Structure of Diatom Ptc6.

A, The conserved and semi conserved amino-acid residues among the seven algal species and two cyanobacterial species are indicated by black and gray boxes respectively. The heme ligands, the residues forming the acidic patch, and the residues forming a salt-bridge are shown in yellow, red, and green respectively. The secondary structures of cyt c_6 of Ptc6 are indicated as follows: orange cylinders, α-helices; blue arrows, β-sheet. B, Overall structure of diatom Ptc6. The α-helix (marine) and β-sheet (green) are indicated using a cartoon model. The amino acid residues, heme group, and sulfate ions are represented by a stick model with atom-specific colors: white, carbon; blue, nitrogen; red, oxygen; yellow, sulfur; iron, orange. C, Superimposion of C^{α} traces of cyts c_6 of diatom *P. tricornutum* (purple; PDB code 3dmi), red alga *P. yezoensis* (red; PDB code 1gdv), green alga *C. reinharditii* (green; PDB code 1cyj), and cyanobacteria *A. maxima* (marine; PDB code 1f1f). D, Salt-bridge of diatom Ptc6. Salt bridge is depicted by a broken line.

Monoraphidium braunii, *Cladophora glomerate*, *Scenedesmus obliquus*, *P. yezoensis*, *Hizikia fusiformis*, *Arthrospira maxima*, and *Phormidium laminosum* revealed identities of 56.7%, 47.19%, 41.76%, 50.6%, 55.7%, 56.7%, 55.6%, and 55.1% respectively (Fig. 2A). The C^{α} trace alignment of cyt c_6 from Ptc6, green alga *C. reinharditii*,[14] red alga *P. yezoensis*,[12] and cyanobacteria *A. maxima*[15] is shown in Fig. 2C. The overall structure of Ptc6 was similar to the structures of algal and cyanobacterial cyt c_6 from red alga *P. yezoensis*,[12] green alga *C. reinharditii*,[14] and cyanobacteria *A. maxima*,[15] with main-chain root mean square deviations of 0.8, 0.6, and 0.6 Å respectively using the DALI program.

A surface exposed salt bridge was formed among Arg44, Asp37, and Glu84 (Arg44NH1-Asp37$O^{\delta 1}$, 2.98 Å, Arg44NH2-Glu84$O^{\varepsilon 2}$, 2.89 Å) (Fig. 2D). Arg44 was conserved only in the diatom cyt c_6 (Fig. 2A), and this salt bridge has not been found in other cyts c_6 in the same region. Considering that a salt bridge of high binding energy contributes to the structural stability of a protein,[16] this salt-bridge of Ptc6 might contribute to the rigid packing of the interaction between helices II and IV and might increase the structural stability of the protein. Gdn-HCl cannot distinguish the contributions of electrostatic interaction such as a salt bridge, but the effects of a salt bridge are effectively monitored in urea, because the urea molecular is uncharged.[17] Urea denaturation experiments indicated that oxidized Ptc6 was more stable than red alga *P. yezoensis* cyt c_6. Hence, this salt bridge of Ptc6 may be one of the factors bringing it about that structural stability of Ptc6 is higher than that of red algal cyt c_6. This prediction is worthy of further study.

In this study, we determined the first crystal structure of diatom cyt c_6 at 1.5 Å resolution. The UV/vis spectra and redox potential of the protein were similar to those of other algal cyts c_6. The structural stability of Ptc6 was higher than that of red algal cyt c_6. Based on the results for crystal structure and for denaturation with urea of Ptc6, we estimated that this structural stability was to be attributed to a salt bridge, which was not found in other cyts c_6, among Arg44, Asp37, and Glu84 around helices II and IV.

Acknowledgment

This work was supported in part by the Nihon University College of Bioresource Sciences Research Fund for 2008.

References

1) Cavalier-Smith, T., Membrane heredity and early chloroplast evolution. *Trends Plant Sci.*, **5**, 174–182 (2000).
2) McFadden, G. I., Plastids and protein targeting. *J. Eukaryot. Microbiol.*, **46**, 339–346 (1999).
3) Peers, G., and Price, N. M., Copper-containing plastocyanin used for electron transport by an oceanic diatom. *Nature*, **441**, 341–344 (2006).
4) Shimazaki, K., Takamiya, K., and Nishimura, M., Studies on electron transfer systems in the marine diatom *Phaeodactylum tricornutum*. I. Isolation and characterization of cytochromes. *J. Biochem.*, **83**, 1631–1638 (1978).
5) Killian, O., and Kroth, P. G., Presequence acquisition during secondary endocytobiosis and the possible role of introns. *J. Mol. Evol.*, **58**, 712–721 (2004).
6) Akazaki, H., Kawai, F., Chida, H., Matsumoto, Y., Hirayama, M., Hoshikawa, K., Unzai, S., Hakamata, W., Nishio, T., Park, S.-Y., and Oku, T., Cloning, expression and purification of cytochrome c_6 from the brown alga *Hizikia fusiformis* and complete X-ray diffraction analysis of the structure. *Acta Crystallogr. F*, **64**, 674–680 (2008).
7) Satoh, T., Itoga, A., Isogai, Y., Kurihara, M., Yamada, S., Natori, M., Suzuki, N., Suruga, K., Kawachi, R., Arahira, M., Nishio, T., Fukazawa, C., and Oku, T., Increasing the conformational stability by replacement of heme axial ligand in *c*-type cytochrome. *FEBS Lett.*, **531**, 543–547 (2002).
8) Lange, C., Hervás, M., and De la Rosa, M. A., Analysis of the stability of cytochrome c_6 with an improved stopped-flow protocol. *Biochem. Biophys. Res. Commun.*, **310**, 215–221 (2003).
9) Pettigrew, G. W., and Moore, G. R., "Cytochromes *c*: Evolutionary, Structural and Physicochemical Aspects," Springer, Berlin, pp. 161–170 (1990).
10) Otwinowski, Z., and Minor, W., Processing of X-ray diffraction data collected in oscillation mode. *Methods Enzymol.*, **276**, 307–326 (1997).
11) Collaborative Computational Project, Number 4, The CCP4 suite: programs for protein crystallography. *Acta Crystallogr. D*, **50**, 760–763 (1994).
12) Yamada, S., Park, S.-Y., Shimizu, H., Koshizuka, Y., Kadokura, K., Satoh, T., Suruga, K., Ogawa, M., Isogai, Y., Nishio, T., Shiro, Y., and Oku, T., Structure of cytochrome c_6 from the red alga *Porphyra yezoensis* at 1.57 Å resolution. *Acta Crystallogr. D*, **56**, 1577–1582 (2000).
13) Emsly, P., and Cowtan, K., Coot: model-building tools for molecular graphics. *Acta Crystallogr. D*, **60**, 2126–2132 (2004).
14) Kerfeld, C. A., Anwar, H. P., Interrante, R., Merchant, S., and Yeates, T. O., The structure of chloroplast cytochrome c_6 at 1.9 Å resolution: evidence for functional oligomerization. *J. Mol. Biol.*, **250**, 627–647 (1995).
15) Sawaya, M. R., Krogmann, D. W., Serag, A., Ho, K. K., Yeates, T. O., and Kerfeld, C. A., Structures of cytochrome *c*-549 and cytochrome c_6 from the cyanobacterium *Arthrospira maxima*. *Biochemistry*, **40**, 9215–9225 (2001).
16) Nakamura, H., Roles of electrostatic interaction in proteins. *Q. Rev. Biophys.*, **29**, 1–90 (1996).
17) Monera, O. D., Kay, C. M., and Hodges, R. S., Protein denaturation with guanidine hydrochloride or urea provides a different estimate of stability depending on the contributions of electrostatic interactions. *Protein Sci.*, **3**, 1984–1991 (1994).

Available online at www.sciencedirect.com
ScienceDirect
Bioorganic & Medicinal Chemistry Letters 18 (2008) 120–123
Bioorganic & Medicinal Chemistry Letters

(2*S*,2′*R*)-Analogue of LG190178 is a major active isomer

Wataru Hakamata,[a] Yukiko Sato,[a] Haruhiro Okuda,[a] Shinobu Honzawa,[b] Nozomi Saito,[b] Seishi Kishimoto,[b] Atsushi Yamashita,[b] Takayuki Sugiura,[b] Atsushi Kittaka[b] and Masaaki Kurihara[a,*]

[a]*Division of Organic Chemistry, National Institute of Health Sciences, Kamiyoga, Setagaya-ku, Tokyo 158-8501, Japan*
[b]*Faculty of Pharmaceutical Sciences, Teikyo University, Sagamiko, Kanagawa 199-0195, Japan*

Received 27 June 2007; revised 17 October 2007; accepted 1 November 2007
Available online 5 November 2007

Abstract—Vitamin D receptor (VDR) ligands are therapeutic agents for the treatment of psoriasis, osteoporosis, and secondary hyperparathyroidism. VDR ligands also show immense potential as therapeutic agents for autoimmune diseases and cancers of the skin, prostate, colon, and breast as well as leukemia. LG190178 is a novel non-secosteroidal ligand for VDR. We synthesized and evaluated stereoisomers of LG190178 and found that only an (2*S*,2′*R*)-analogue of LG190178 (YR301) had strong activity.

The active form of vitamin D_3, 1α,25-dihydroxyvitamin D_3 (1α,25-$(OH)_2D_3$), is not only a regulator of calcium homeostasis and bone development and remodeling but also a potent differentiator of leukemic cells. 1α,25-$(OH)_2D_3$ and its synthetic analogues exert these effects by binding to the vitamin D receptor (VDR) which belongs to the steroid/thyroid hormone nuclear receptor superfamily. The X-ray crystal structure of the ligand binding domain (LBD) of VDR with 1α,25-dihydroxyvitamin D_3 was determined by Moras et al. in 2000 and the binding mode between ligands and LBD-VDR was revealed.[1] This enables the design of VDR ligands by structure-based drug design. We have also designed secosteroidal analogues[2] (Fig. 1).

Recently, non-secosteroidal ligands for VDR have been an attractive target for the development of new therapeutics.[3] LG190178 is the first novel non-secosteroidal ligand, with potential as therapeutic for cancer, leukemia, and psoriasis with less calcium mobilization side effects than are associated with secosteroidal 1α,25-$(OH)_2D_3$ analogues,[4] however, LG190178 includes four stereoisomers.[5] We calculated to make ducking model of four isomers and VDR, respectively,[6] and the results are summarized in Figure 2 and Table 1. The (2*S*,2′*R*)-isomer model was the most stable. There were hydrogen bonds between 2-OH and Arg-274, Ser-237 and between 2′-OH and His-305, His-397. (2*S*)-Isomers ((2*S*,2′*S*) and (2*S*,2′*R*)) are expected to be more important than (2*R*)-isomers.

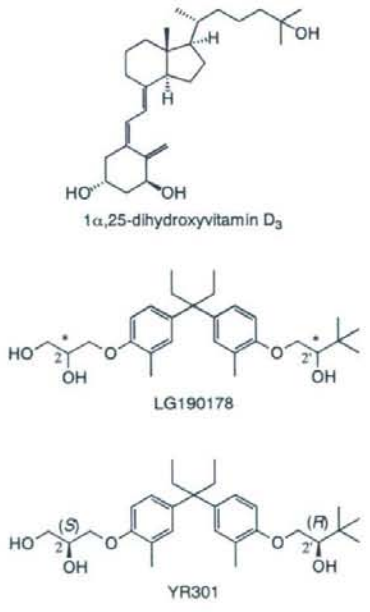

Figure 1. Structure of 1α,25-dihydroxyvitamin D_3, LG190178, and YR301.

Keywords: Vitamin D receptor; Non-secosteroidal ligand; (2*S*,2′*R*)-LG190178; YR301.
* Corresponding author. E-mail: masaaki@nihs.go.jp

0960-894X/$ - see front matter © 2007 Elsevier Ltd. All rights reserved.
doi:10.1016/j.bmcl.2007.11.007

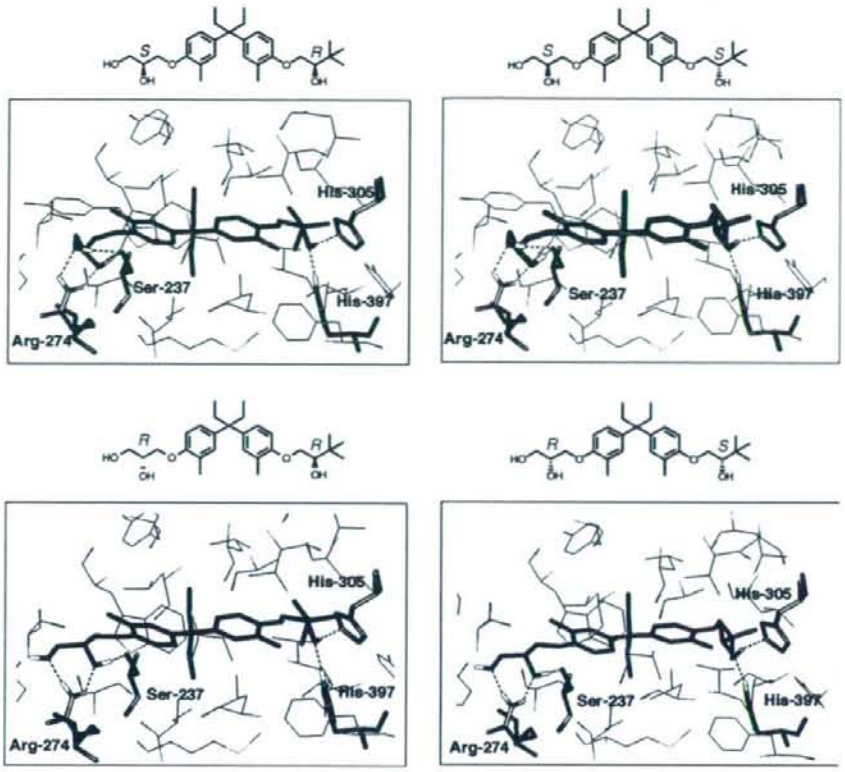

Figure 2. Modeled structure of stereoisomers of LG190178 bound to VDR.

Table 1. Difference of potential energy of docking modeling of four isomers and VDR

Model	AE (kcal/mol)
I (2*S*,2′*R*)	0
II (2*S*,2′*S*)	+1.87
III (2*R*,2*R*)	+3.56
IV (2*R*,2′*S*)	+4.94

We synthesized (2*S*)-LG190178 and (2*R*)-LG190178. The synthetic routes of (2*S*)-isomers and (2*R*)-isomers are shown in Scheme 1. The 2-position asymmetric center was constructed using optically active glycidols. (2*S*)-Analogues and (2*R*)-analogues were analyzed by HPLC with a chiral column (CHIRALPAK IA, solvent: hexane/EtOH 9:1). HPLC charts are shown in Figure 3. The four isomers are YR301, YR302, YR303, and YR304, respectively. To determine the stereochemistry of the 2′-position, we synthesized the (2*S*,2′*R*)-isomer from (*R*)-diol **6**. (*R*)-1-(Benzyloxy)-3,3-dimethylbutan-2-ol **5** was separated using HPLC with a chiral column (CHIRALPAK IA, DAICEL; solvent: hexane/EtOH 9:1) and hydrogenated in the presence of $Pd(OH)_2/C$ to afford compound **6** ($[\alpha]_D^{25}$ −31.6 (*c* = 1.00, methanol)) in 70% yield. Absolute configuration of **6** was determined by comparing the optical rotation of **6** with that of the literature.[7] Scheme 3 shows the synthesis of the (2*S*,2′*R*)-isomers from (*R*)-diol **6**. Then YR301 was determined to be the (2*S*,2′*R*)-isomer. Using the same procedures YR302, 303, and 304 were determined to be (2*S*,2′*S*)-isomer, (2*R*,2′*R*)-isomer, and (2*R*,2′*S*)-isomer, respectively (Scheme 2).

Isomers were examined for transcriptional assays and VDR affinity. The results are summarized in Table 2. (2*S*,2′*R*)-Isomer (YR301) exhibited potent transcriptional activity, comparable to natural ligand 1α, 25-$(OH)_2D_3$. Moreover, in the cases of human colon carcinoma cell, YR301 exhibited stronger activities than 1α,25-$(OH)_2D_3$. (2*S*,2′*S*)- and (2*R*,2′*R*)-isomers, diastereomers of (2*S*,2′*R*), decreased the activity by two orders of magnitude, compared with (2*S*,2′*R*)-isomer (YR301). (2*R*,2′*S*)-Isomer, the enantiomer of (2*S*,2′*R*) exhibited the weakest activity. It is very interesting that only YR301 showed strong activity. Figure 4 shows an overlay of the X-ray structure of 1α,25-$(OH)_2D_3$ and modeled structure of (2*S*,2′*R*)-isomer (YR301) in LBD of VDR. YR301 is well overlapped with 1α,25-$(OH)_2D_3$, especially with the hydrophobic region, but YR301 is not expected to be H-bonded to Tyr-143 and Ser-278, which are H-bonded to 1α,25-$(OH)_2D_3$. It is important to remember that considering H-bonds to Tyr-143 and Ser-278 is important in the design of new ligands.

In summary, we revealed that YR301, an (2*S*,2′*R*)-analogue of LG190178, was a major active isomer. YR301

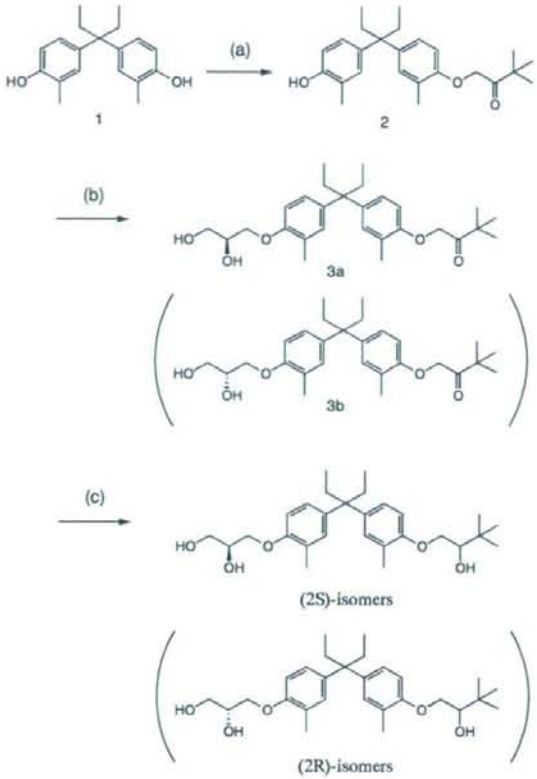

Scheme 1. Reagents and conditions: (a) $ClCH_2CO^tBu$, NaH, DMF, 80 °C, 12 h, 40%; (b) (*S*)-glycidol (or (*R*)-glycidol), NaH, DMF, 80 °C, 3 h, 59%; (c) $NaBH_4$, MeOH, rt, 2 h, 89%.

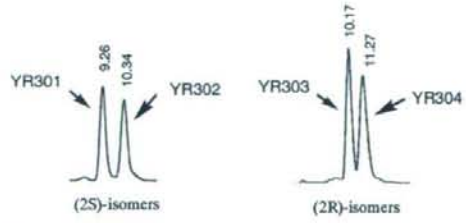

Figure 3. HPLC chart.

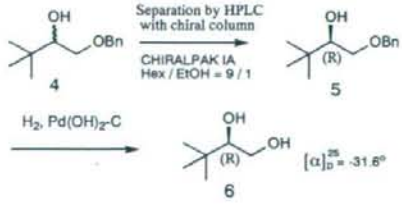

Scheme 2. Separation and determination of chiral.

exhibited potent biological activity, comparable to natural ligand 1α,25-$(OH)_2D_3$. Non-secosteroidal ligands for VDR are novel candidates for therapeutic agents.

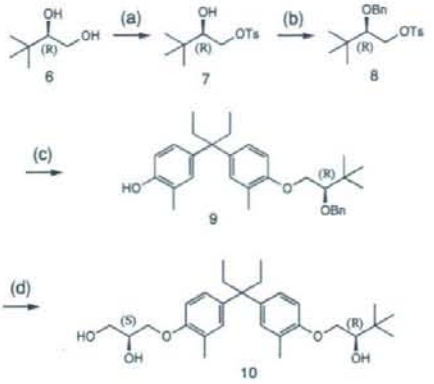

Scheme 3. Reagents and conditions: (a) TsCl, C_5H_5N, CH_2Cl_2, rt, 19 h, 52%; (b) benzy trichloroacetimidate, TMSOTf, DMF, rt, 5 h, 72%; (c) **1**, NaH, DMF, rt, 1 h, 32%; (d) (*S*)-glycidol, NaH, DMF, 80 °C, 3 h, 43%; H_2, $Pd(OH)_2$/C, rt, 24 h, 93 h.

Table 2. Biological activities for transcriptional assays and VDR affinity

Compound	Transcription EC_{50} (nM)			VDR affinity
	HOS/SF[a]	HOS/5% FCS[b]	Caco-2/5% FCS[c]	
1α,25$(OH)_2D_3$	0.0106	0.555	3.52	100
YR301 (2*S*,2′*R*)	0.0396	0.79	1.80	28.3
YR302 (2*S*,2′*S*)	1.66	9.9	21.1	0.831
YR303 (2*R*,2′*R*)	4.68	16.8	22.1	0.482
YR304 (2*R*,2′*S*)	15.6	83.2	131.4	0.112

[a] Human osteosarcoma cell, serum free.
[b] Human osteosarcoma cell, 5% fetal calf serum.
[c] Human colon carcinoma cell, 5% fetal calf serum.

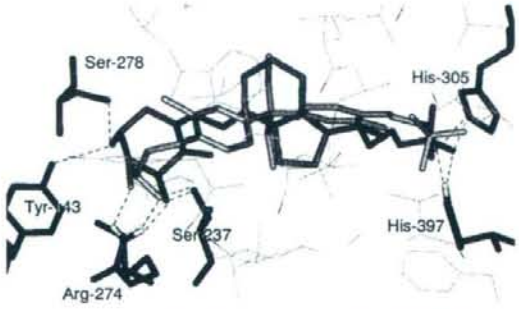

Figure 4. Overlay of the X-ray structure of 1α,25-$(OH)_2D_3$ and modeled structure of YR301 in VDR. 1α,25-$(OH)_2D_3$ and YR301 are shown in orange and green, respectively. Hydrogen bonds are drawn as dotted lines.

Acknowledgments

This work was supported in part by the Budget for Nuclear Research of the Ministry of Education, Culture, Sports, Science, and Technology, based on the screening and counseling by the Atomic Energy Commission and by a Grant-in-Aid for Scientific Research (C) from the Japan Society for the Promotion of Science.